Ion Stopping in Dense Plasma Target for High Energy Density Physics

C. Deutsch[*,1], G. Maynard[1], M. Chabot[2], D. Gardes[2], S. Della-Negra[2], R. Bimbot[2], M.F. Rivet[2], C. Fleurier[3], C. Couillaud[4], D.H.H. Hoffmann[5], H. Wahl[5], K. Weyrich[5], O.N. RosmeJ[5], N.A. Tahir[5], J. Jacoby[6], M. Ogawa[7], Y. Oguri[7], J. Hasegawa[7], B. Sharkov[8], A. Golubev[8], A. Fertman[8], V.E. Fortov[9] and V. Mintsev[9]

[1]*LPGP (UMR-CNRS 8578) Université Paris XI, 91405 Orsay, France*

[2]*IPN (CNRS-IN2P3), Université Paris XI, 91405 0rsay, France*

[3]*GREMI (UMR-CNRS 6606) Université d'Orléans, Orleans, France*

[4]*CEA-DAM, BP 12, 91680 Bruyeres-le-Chatel, France*

[5]*GSI, Plasmaphysik, Planck Str. 1, D-64291 Darmstadt, Germany*

[6]*Goethe-Universitat, von Laue Str. 1, D-60438 Frankfurt, Germany*

[7]*RNLR-TIT Ohokayama, Meguro-Ku, Tokyo 152-8550, Japan*

[8]*ITEP, Cheremushkinskaya 25, 117218 Moscow, Russia*

[9]*IHED, Izhorskaya 13/19, 125412 Moscow, Russia*

Abstract: The basic physics of nonrelativistic and electromagnetic ion stopping in hot and ionized plasma targets is thoroughly updated. Corresponding projectile-target interactions involve enhanced projectile ionization and coupling with target free electrons leading to significantly larger energy losses in hot targets when contrasted to their cold homologues.

Standard stoppping formalism is framed around the most economical extrapolation of high velocity stopping in cold matter. Further elaborations pay attention to target electron coupling and nonlinearities due to enhanced projectile charge state, as well.

Scaling rules are then used to optimize the enhanced stopping of MeV/amu ions in plasmas with electron linear densities nel ~ 10^{18}-10^{20} cm^{-2}.

The synchronous firing of dense and strongly ionized plasmas with the time structure of bunched and energetic multicharged ion beam then allow to probe, for the first time, the long searched enhanced plasma stopping and projectile charge at target exit.

Laser ablated plasmas (SPQR1) and dense linear plasma columns (SPQR2) show up as targets of choice in providing accurate and on line measurements of plasma parameters.

Corresponding stopping results are of a central significance in asserting the validity of intense ion beam scenarios for driving thermonuclear pellets. Other applications of note feature thorium induced fission, novel ion sources and specific material processing through low energy ion beams.

Last but not least, the given ion beam-plasma target interaction physics is likely to pave a way to the production and diagnostics of warm dense matter (WDM).

1. INTRODUCTION

From time to time, significant review articles dedicated to charged particle stopping in cold matter (gas or solid) with electrons bound in atoms and molecules have appeared a number of time [1, 2]. Those works mainly pertained to electromagnetic coupling (mostly electrostatic) between cha- rged projectiles and a given target. Corresponding investigations stand as obvious prerequisites to those devoted to much stronger hadron-hadron coupling for nuclear and particle studies.

In this perspective, it does not seem to make much of a difference, whether the target electrons remain bound or get ionized and then move freely within target.

However, the recent and sustained interest of accelerator physicists for inertial confinement fusion (ICF) through intense heavy ion beams at one-third speed light (E/A ~

*Address correspondence to this author at the LPGP (UMR-CNRS 8578) Université Paris XI, 91405 Orsay, France; Tel: 331 6915 7605; Fax: 331 6915 7844; E-mail: claude.deutsch@pgp.u-psud.fr

50 MeV/a.m.u.) has recently dramatically increased a general concern for ion stopping in ionized and plasmalike targets [3, 4].

Accelerator physicists are also strongly attracted to the potentialities offered by well taylored discharge (Z pinch for instance) plasmas as particle beam strippers, focussing lenses, beam dump and more.

A closely related area of endeavor concerns the *in situ* production of relativistic electron and ion beams [5] in precompressed thermonuclear pellets through femtosecond lasers and intense ion beams carrefully time sequenced. Finally, it is also worthwhile mentioning that the interaction of very swift ions with dilute and ionized interstellar matter stands as an absolute prerequisite to understanding the transport of cosmic ray particles throughout space [6].

The interaction of ion beams with dense and fully ionized plasmas has recently been promoted as a major area for investigation [7-11]. It lies at the border of atomic and discharge physics. These topics are of a crucial significance in asserting the feasibility of manipulating intense beams of light or heavy ions towards compressing hollow microspheres (a few hundred microns in diameter) up to ignition of the deuterium + tritium fuel delivering α particle and neutron thermonuclear yields.

The basic mechanisms underlying the physics of charged particles stopping in various states of matter have been the subject of intense scrutiny since the very early days of quantum mechanics. Since then, electromagnetic coupling between projectiles and target particles has always been the topic of ever increasingly sophisticated approaches. As a result, we now have a very large body of data for stopping ions in a neutral target.

However, all these studies were invariably conducted with an electrically neutral target material. Recently, the consideration of fully ionized targets, composed of ions and electrons, has emerged as a novel challenge with major concerns for thermonuclear research, high-energy particle acceleration and related fields of interest.

For many years ion-plasma interactions were encountered in a variety of situations of technological and engineering concern. A conspicuous example is thus afforded by the intense deuterium ion beams in the 500-800 keV energy range, routinely used for additional heating of tokamaks and other magnetically confined plasmas. However, the specific issues associated with the basic physics of ion beam stopping in a strongly ionized plasma medium was never considered a topic of fundamental interest.

This situation changed quite abruptly at the beginning of the 1980s with the emerging possibilities of achieving inertial compression of hollow spheres, a few millimeters in diameter, containing the deuterium + tritium thermonuclear fuel through energetic and intense light ion or heavy ion beams.

Considered intensities are in the MA cm^{-2} range for light ions (D^+ or Li^+ at a few MeV/nucleon) and in the 10 kA cm^{-2} range for heavy ions ((B_i^+ , U^{n+} at 50 MeV/nucleon). Then, suddenly, the basic physics of ion stopping in dense plasmas

got pushed ahead to the forefront of interest of many physicists, in view of its unavoidable relevance in assessing the basic trends of driver-pellet interaction. Otherwise specified atomic units (au) are used in the sequel.

The present review is structured as follows.

In Sec. 2, we ground the interaction of intense ion beams with cold and hot targets on the so-called reduction principle. This latter advocates a neglect of any intrabeam correlation, so the ion beam-target interaction may be safely restricted to a much simpler single ion-target one.

Corresponding theoretical expectations are then carefully elaborated in Sec. 3 with ion-plasma interaction framed within the so-called standard stopping model (SSM) established on a beam-target parameter analysis. General SSM trends are identified. A central concept of enhanced plasma stopping (EPS) is unambiguously demonstrated for plasma targets of interest for inertial confinement fusion (ICF). The, the ion projectile-target electron interaction may be treated within framework of the Born-RPA approximation. Nonlinear (strong coupling…) corrections improving the SSM are also considered.

The experimental consequences of the theoretical analysis are outlined in Sec. 4 through relevant scaling laws. The resulting instrumental methodology is discussed in Sec. 5. It advocates a synchronous firing of the target plasma with the ion beam time structure. Energy loss at high projectile velocity is then substantially documented in Secs. 5 and 6. Low velocity stopping is discussed in Sec. 7. Specific features of MeV proton beams interacting with fully ionized hydrogenic plasmas are documented in Sec. 8. The possibility of directly heating a plasma target through intense ion beam impact is investigated in Sec. 9. Sec. 10 is devoted to a summary and conclusions are also offered therein.

2. REDUCTION PRINCIPLE

One of the misconceptions which seems to have prevented physicists addressing earlier the issues of charged particle stopping in dense plasmas, was the prejudice that an inferno of collective plasma effects would occur and blur out the basic mechanisms associated with the ion beam-plasma interaction itself.

Such expectations are unfortunately fulfilled by the interaction of intense electron beams with dense plasmas, which explain why they are considered useless for inertial confinement fusion (ICF) when used as a primary driver. On the other hand, it has been documented recently through a lot of numerical simulations and adequately designed experiments that this deleterious collective behaviour takes only a virtually negligible energy toll during the ion-plasma interaction.

This latter effect can thus be safely reduced to a linear superposition of single ion stopping in a hot medium mostly constituted of free electrons.

Such a fortunate occurrence is straightforwardly based on a very simple argument. Actually, as far as the most intense ion beams are considered for ICF purposes, the mean interior distance remains, at least, two orders of magnitude above the electron screening length in the considered dense plasma

targets. The same situation also prevails for the cold target exposed to the incoming ion beam.

All heavy-ion fusion (HIF) scenarios claim that current densities up to 10 kA/cm^2 are required to achieve a break-even. Nevertheless, even under these unusual conditions, the average ion-ion distance in the beam remains much larger than the electron fluid screening lengths. These latter are deduced either from Debye-Hückel theory with

$$\lambda_D (cm) = 6.90 \left[\frac{T(K)}{n(cm^{-3})} \right]^{1/2} \quad , \ k_B T \gg E_F$$

and the Fermi energy

$$E_F = \frac{1.84}{r_S^2} \ , \qquad r_S = \left[\frac{3}{4\pi n_e} \right]^{1/3} a_0^{-1} \ , \ a_0 = \text{Bohr radius}$$

or from the Thomas-Fermi expression $\sim (0.611 r_S)^{1/2}$ at low enough temperature. These data always remain much smaller than the ion interparticle distances in beams considered for HIF.

These simple considerations allow us to reduce the beam-target interaction to an ion-target one, by neglecting collective aspects in a first approach. In so doing, we have built the contents for the so-called reduction principle. This welcome simplification should nevertheless be taken with some reservations for the case of protons. The corresponding current densities may well range up to MA/cm^2, so that some caution should be exercised in every practical situation dealing with light ion beams.

With these minor restrictions taken into account, one is entitled to make use of conventional wisdom as to which intense beams are likely to appear dilute in the target. Had we considered intense electron beams, the collective phenomena would not have been so easily eliminated. For instance, potential wells can develop in the plasma produced by heating a thin foil, se that incoming projectiles are likely to be trapped and accelerated backward after several bouncing periods.

So, if the ion beams are not submitted to filamentation instability, which can reduce drastically the mean ion relative distance, the projectiles do not see each other while stopping in dense matter. The reduction principle allows for a very efficient simplification of the interaction of intense atomic ion beams with a dense target.

3. BASIC THEORY

3.1. Parameter Analysis

A basic understanding of the stopping of nonrelativistic and multicharged ions in a ionized medium requires a preliminary and carefull identifications of a number of dimensionless parameters. Such a procedure is mandatory in order to frame realistically projectile-target coupling in a spirit germane to standard kinetic theory [14] in agreement with the observation that a stopping power quantity features essentially a transport coefficient.

Physically pertinent observables obviously include projectile velocity v_b (nonrelativistic), its charge state Z_p, usually a v_b-dependent quantity, target electron density n_e

(free and bound) and target ionization degree, and also target plasma parameter (ratio of potential Coulomb to kinetic energies).

Detailed analysis proceeds as usual through a full-fledged hamiltoniant formalism, detailed elsewhere [12-14].

As in cold matter, a first relevent parameter is featured by the so-called Born parameter $\eta_B = \frac{Z_p}{V_p}$ (in atomic units), or $\frac{Z_p c}{137 V_p}$ otherwise explicitly in terms of speed light c. Most of ion beam-plasma interaction experiments performed up to now lie in the realm of the Born-RPA approximation with $\eta_B \ll 1$ [12].

The present analysis essentially stresses ion stopping through inelastic interactions with target electrons, which are playing an over important role compared to target ions for projectile energies between 0.1 MeV/a.m.u and 1 GeV/a.m.u.

For discussing the energy loss at strong target coupling we thus consider mainly a pointlike projectile of given charge in a free electron target plasma [13, 15]. This restriction to free electrons becomes of course more and more realistic for increasing degrees of ionization, that is at high temperatures. Also in dense plasmas bound states disappear through a lowering of the continuum edge. For investigations concerning electron cooling of ion beam (emittance reduction) even the real target is a free electron target [14].

The key observable in experiments exploring the interaction of charged particles with matter is usually the energy loss ΔE of the projectile ion. It is obtained by comparing the kinetic energy of the ion before and after passing through the target. A more detailed quantity is the stopping power which is defined as the energy change per unit path-length dE/ds and which corresponds to the actual decelerating force on the ion.

The stopping power can be directly derived from the energy loss per path length as dE/ds(v) = $\Delta E/\Delta s$ provided ΔE and Δs remain sufficiently small, as it is often the case for experiments with heavy projectiles and thin targets as well as for simulation studies.

For most theoretical approaches the stopping power is more conveniently defined either by the change of its kinetic energy

$$dE / ds = \frac{1}{v} \frac{d}{dt} \left\langle \mathbf{P}^2 / 2M \right\rangle \tag{1}$$

or by the decelerating force as the change in the momentum of the projectile projected on the direction of motion

$$dE / ds = \frac{\mathbf{v}}{v} \cdot \mathbf{F} = \frac{\mathbf{v}}{v} \cdot \frac{d}{dt} \left\langle \mathbf{P} \right\rangle . \tag{2}$$

Both definitions are equivalent if the projectile travels along a straight line as it is the case for sufficiently high projectile energies and/or large masses. Difficulties show up at very low projectile energy mean kinetic energy when projectile thermalize in target through a kind of Brownian motion with stochastically changing momenta. We concentrate now on the proper deceleration processes where

the ion travels along a straight or smoothly varying path. This allows for a clearcut definition of a stopping power.

The energy loss of an ion impinging on an electron target plasma is determined by the direct interaction of the ion with the target electrons and by the interparticle correlations within the target. Hence, it is necessary to characterize the ion-target system in two respects first, concerning the strength of the ion-target coupling, and second, concerning the electron-electron correlations in the plasma target. Ideality parameter ξ for the electron plasma is introduced as the ratio of the mean potential energy E_{pot} of the electron interaction to the mean kinetic energy E_{kin} of the electrons. The first one can be estimated by the potential energy for two electrons separated by distance $a=(4\pi n/3)^{-1/3}$, the Wigner-Seitz radius for an electron density n. Mean kinetic energy, $E_{kin}=E_F+k_BT$ interpolates between Fermi-energy E_F for a fully degenerate plasma with temperature T = 0 and thermal energy k_BT for a hot, nondegenerate plasma. Target electron coupling is thus featured as [14]

$$\xi = \frac{E_{pot}}{E_{kin}} = \frac{e^2}{4\pi\varepsilon_0 a(E_F + k_BT)} = \frac{2\alpha^2 r_s}{1+\Theta}, \qquad (3)$$

where $r_s = a/a_0$, and $\alpha = (4/9\pi)^{1/3} = 0.521$ … For small $\xi \ll 1$ the behavior of the electron plasma is dominated by the kinetic energy of the electrons and we are in an ideal, collisionless regime where collective plasma phenomena prevail. Increasing $\xi \geq 1$ corresponds to a strongly coupled, nonideal electron plasma with increasing contribution of interparticle correlations to thermodynamic equilibrium.

The definition of ξ also involves the degree of degeneracy

$$\Theta = \frac{k_BT}{E_F} = \frac{k_BT}{13.6\,eV}(\alpha r_s)^2 \qquad (4)$$

ratio of thermal energy $k_BT = mv_F^2$ to Fermi energy $E_F = mv_F^2/2$.

Θ accounts for the Pauli repulsion. Electrons obeying Fermi-Dirac statistics for $\Theta \ll 1$ can be treated classically within Boltzmann statistics for $\Theta \gg 1$. For nondegenerate plasma, $\Theta \gg 1$, the parameter of ideality ξ becomes identical to the classical plasma parameter Γ

$$\Gamma = \frac{e^2}{4\pi\varepsilon_0 a k_BT} = \frac{2\alpha^2 r_s}{\Theta} \xleftarrow{1\ll\Theta} \xi . \qquad (5)$$

Coulomb parameter $\eta_e = \dfrac{e^2}{4\pi\varepsilon_0 \hbar v_r}$ highlights the quantum mechanical wave nature of the interacting electrons. Replacing relative velocity v_r, by the averaged relative velocity $\langle v_{ee}\rangle$ between two target electrons we get the averaged Coulomb parameter

$$\eta_e = \frac{e^2}{4\pi\varepsilon_0 \hbar \langle v_{ee}\rangle} \xrightarrow{\Theta\gg1} \sqrt{\frac{13.6eV}{k_BT}}, \qquad (6)$$

with dimensionless relative velocity $\langle v_{ee}\rangle' = \langle v_{ee}\rangle/\langle v_e\rangle$ scaled in units of the averages single electron velocity $\leq v_e>$. The more specific $\langle v_{ee}\rangle = 2^{1/2}\langle v_e\rangle$ can be derived in the limit of a nondegenerate plasma ($\Theta >1$) with a Maxwell velocity distribution. Classical motion is a good approximation if $\eta_e, \langle\eta_e\rangle \gg 1$ while a quantum mechanical treatment is requested for $\eta_e, \langle\eta_e\rangle < 1$.

There the ion charge state has to remain small compared to the number N_D in a Debye sphere or, more precisely, to the number $N_D(1+(v/v_{th})^2)^{3/2}$ in the dynamical screening sphere in order to insure that each electron contributes only slightly to the screening or, more generally, to the target response.

Up to now, we mosly restricted attention to the target electron component, implicitly assuming a neutralizing charge background behavior for the ion component. However, if one focusses on small Γ (<1) targets, the most often considered ones experimentally, the above discussion may be nearly verbatim transferred to the ion component by replacing electron parameters by ion ones. Moreover, we also implicitly assumed a fixed projectile charge Z_b, while it is well-known to be a v_b-dependent quantity.

3.2. Standard Stopping Model (SSM)

First, let us consider a binary interaction between a pointlike ion projectile and plasma particles, also taken as pointlike, equivalent to a full quantum-mechanical description. The given pointlike-pointlike interaction obviously pertains to a high temperature plasma target with classical particles, and also to a sufficiently dense degenerate electron jellium with a kinetic temperature T below the corresponding Fermi temperature T_F. In the latter case, the target electrons experience a long range Coulomb repulsion altogether with a short range Pauli repulsion due to the exclusion principle increasing with degeneracy ratio T_F / T [13].

Then, a fruitful technical contact may be achieved with standard notations barrowed from low-temperature ($T \ll T_F$) condensed matter physics. Let us consider a homogeneous electron fluid (jellium) with uniform particle density n. It is then appropriate to measure interparticle distance in terms of Bohr radius $a_0 = \hbar^2 / m_e e^2 = 0.529\text{Å} \equiv 1$ atomic unit (au) and the dimensionless Wigner parameter r_S fulfilling

$$\frac{4\pi r_S^3}{3} = \left(n\, a_0^3\right)^{-1},$$

volume of the Wigner-Seitz cell per electron. It is also useful to introduce the Lindhard-Winter ratio of potential to kinetic energy

$$\chi^2 \equiv \frac{e^2}{\pi\hbar V_p} = \frac{r_S}{6.02}$$

with

$$V_F = \frac{1.919}{r_S} \text{ au}, \text{ Fermi velocity}$$

and the velocity unit (a.u)

$$V_0 = \frac{e^2}{\hbar} = 2.18\times10^8 \text{ cm / sec}.$$

The Fermi energy $E_F = \frac{V_F^2}{2}$ $(m_e = 1)$ is then $\frac{1.84}{r_s^2}$ a.u and the plasmon energy is $\omega_p = \frac{\sqrt{3}}{r_s^{3/2}}$.

Fig. (**1**) depicts in the temperature-density plane most of target plasmas of present concern envisionned in inertial confinement fusion (ICF) and magnetically confined fusion (Tokamaks) as well. They are contrasted to several solar plasmas. Despites a dispersion on a wide range of parameters magnitude, those plasmas share a common weak coupling $T = 0$ ratio $\chi^2 = \frac{\alpha' r_s}{\pi} \ll 1$ with $\alpha' = \left(\frac{9\pi}{4}\right)^{-1/3} = 0.5211$.
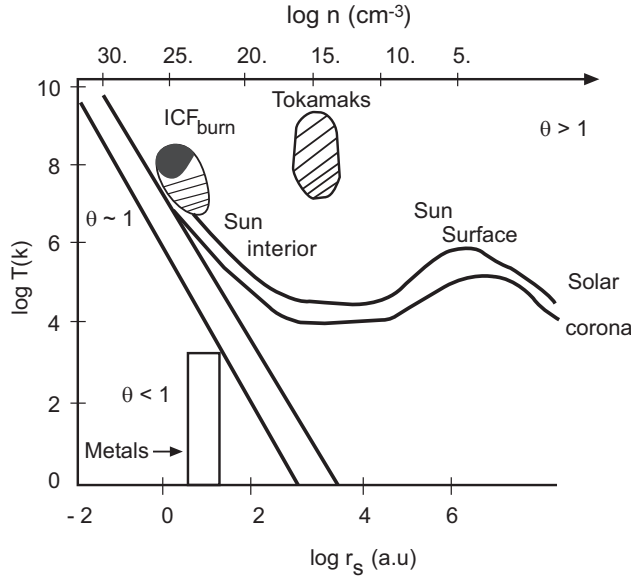
Fig. (1). Plasma map. Density-temperature plane featuring a few salient hot temperature plasmas [Courtesy Anita Brandt].

They are parametrized with respect to electron degeneracy through $\theta = \frac{k_B T}{E_F}$, screening length

$$\lambda_S = \frac{\left[(k_B T)^2 + \left(\frac{2}{3} E_F\right)^2\right]^{1/4}}{\omega_p} ,$$

and coupling parameter

$$\Lambda = \frac{e^2}{\lambda_S \left(k_B T + \frac{2}{3} E_F\right)}$$

with classical $(T \to \infty)$ and quantum $(T \to 0)$ limits included.

As a first and decisive step toward establishing the fundamentals of ion energy loss, we restrict first to a classical electron target. Then, we find it useful to start with a very simple and elegant remark due to Bohr [16] and Fermi [17]. So, we consider a high velocity but nonrelativistic projectile on a rectilinear trajectory with a fixed pointlike charge Z_p at a constant velocity V_p. It can transfer to a target electron the energy

$$\Delta E = \frac{(\Delta q)^2}{2 m_e} , \tag{7}$$

pertaining to the exchanged momentum

$$\Delta q = \int F_\perp dt = \frac{Z_p b e^2}{b^2 V_p} ,$$

in a classical binary collision with impact parameter b, shortest distance between the electron location and projectile trajectory with a force component $F_\perp$ normal to it.

Summing over every available target electron in a cylindrical corona of thickness db with the average $n \int 2\pi b$ db yields at once the average energy loss per unit length

$$\langle \Delta E \rangle = \frac{\pi \left(Z_p e^2\right)^2 n}{m_e V_p^2} \ln \frac{b_{max}}{b_{min}} , \tag{8}$$

which already makes to appear the backbone of high velocity ion stopping in any kind of cold target provided we can fix the impact parameters ratio $\frac{b_{max}}{b_{min}}$. The generality of the derivation leading to Eq. (8) demonstrates that the latter can be considered as a convincing candidate for the stopping paradigm we are looking for.

If ℓ denotes the projection of the projectile trajectory on its target entrance velocity, then we can systematize as shown on Table **1**, the content of the present modelling of ion stopping.

First, we implicity assume that the beam interparticle ion-ion distance should remain much larger than any target distance of significance for the projectile ion-target electron coupling (Table **1**).

Table 1. Stopping Standard Model: Basic Facts and Assumptions [18]

- Intense ion beams appear *dilute* in target
- Rectilinear trajectories
- Pointlike projectiles
- Nonrelativistic regime ($\beta < 0.35$), $\beta = V_p/c$
- $n_e \ell$-scaling $-\Delta E/E = n\ell/E^2$
- Prefactor $4\pi Z_i^2 e^4 n / m_e V_p^2$ dominant for E/A between 1 MeV/amu and 1 GeV/amu
- Log terms dominant at very small (end-of-range) and very large projectile velocity

Next, the purely electromagnetic picture displayed by Eq. (8) clearly demonstrates that the incoming projectile mass has no part in it and also that the same coupling with target ion should produce a result smaller by a factor $\leq \frac{m_e}{m_p} = \frac{1}{1836}$.

In particular, the ion projectile-target ion coupling could decay even more dramatically in a strongly ionized plasma of nonhydrogenic material.

This feature underlies the present restriction of the target to its electron component. The stopping contribution due to the ion component appears as nonnegligible only at very low velocity V_p.

The average energy loss (8) obviously advocates for the scaling law

$$\frac{\Delta E}{E} = \frac{n\ell}{E^2}, \qquad (9)$$

of considerable experimental significance, in terms of the target linear density $n\ell$ (fluence) and projectile kinetic energy E. Paying a specific attention to further ICF applications, we see that the corresponding domain on the density-temperature diagram features $\Gamma \ll 1$. So, the corresponding electron fluid remains weakly coupled and we are entitled to expect a more flexible target.

Up to now, we have essentially framed with our SSM modelling the projectile ion-target electron interaction around a kind of Bethelike regime without paying much attention to the collective plasma aspects of the target.

3.3. Energy Loss at Finite Temperatures (RPA)

We now consider the free electron contributions to the stopping. This is the first term in the complete superposition

$$\frac{dE}{dx} = \sum_i \alpha_i + \sum_j \beta_j + \gamma$$

while β_j and γ denote respectively the bound electrons and the residual ions contribution.

A comprehensive treatment of the energy-loss problem, in terms of the equilibrium dielectric function $\varepsilon(q,\omega)$, can be formulated by starting from the scattering rate [13]

$$R(\vec{q},\omega) = \left(\frac{4\pi Z e^2}{q^2}\right)^2 \frac{2\pi}{\hbar^2} S(\vec{q},\omega) \qquad (10)$$

for energy transfer $\hbar\omega = E(\vec{p}') - E(\vec{p})$ and momentum transfer $\hbar\vec{q} \equiv \vec{p}' - \vec{p}$, which applies to the scattering of a particle of charge $Z_p e$, with initial momentum $\vec{p}$ and energy $E(\vec{p})$, to the final state given by $\vec{p}'$, $E(\vec{p}')$. The dynamical structure factor $S(\vec{q},\omega)$ is related to the dielectric function $\varepsilon(\vec{q},\omega)$ through

$$S(\vec{q},\omega) = \frac{\hbar q^2}{4\pi^2 e^2} N(\omega) \operatorname{Im}\left(\frac{-1}{\varepsilon(q,\omega)}\right), \qquad (11)$$

where $N(\omega) \equiv [\exp(\beta\hbar\omega) - 1]^{-1}$ and $\beta = 1/k_B T$.

The temperature dependence is contained in the dielectric function $\varepsilon(\vec{q},\omega)$ and in the Planck function $N(\omega)$. The energy-loss rate is given by

$$\frac{dE}{dt} = \int \frac{d^3\vec{p}'}{(2\pi\hbar)^3} \hbar\omega R(\vec{q},\omega) \qquad (12)$$

$$= \left(\frac{Z e}{\pi}\right)^2 \int d^3q \frac{\omega N(\omega)}{q^2} \operatorname{Im}\left(\frac{-1}{\varepsilon(\vec{q},\omega)}\right),$$

where $\omega \equiv \omega(\vec{p},\vec{q})$ is determined from

$$\hbar\omega(\vec{p},\vec{q}) \equiv E(\vec{p}') - E(\vec{p}) = \hbar\vec{q}.\vec{v}_p + \frac{\hbar q^2}{2M}$$

in terms of the incident velocity $\vec{v}_p = \frac{\vec{p}}{M}$ and the mass M of the projectile. For heavy particles $M \gg m$, recoil effects are

small and we can expand Eq. (12) in terms of $\Delta\omega \equiv \frac{\hbar q^2}{2M}$ to obtain

$$\frac{dE}{dt} = \left(\frac{dE}{dt}\right)_0 + \left(\frac{dE}{dt}\right)_1 + \dots,$$

where the first two terms are

$$\left(\frac{dE}{dt}\right)_0 = \left(\frac{Z_p e}{\pi}\right)^2 \int d^3q \frac{\omega N(\omega)}{q^2} \operatorname{Im}\left(\frac{-1}{\varepsilon(q,\omega)}\right)\Bigg|_{\omega=\vec{q}.\vec{v}_p} \qquad (13)$$

$$\left(\frac{dE}{dt}\right)_1 = \left(\frac{Z_p e}{\pi}\right)^2 \frac{\hbar}{2M} \int d^3q \frac{\partial}{\partial\omega}\left[\omega N(\omega) \operatorname{Im}\left(\frac{-1}{\varepsilon(q,\omega)}\right)\right]\Bigg|_{\omega=\vec{q}.\vec{v}_p} \qquad (14)$$

The integrals range over both negative frequencies (*loss processes*) and positive frequencies (*gain processes*), but it is here more instructive to transform them into integrals over positive frequencies only.

We can simplify the expression for the main term $(dE/dt)_0$ (Eq. (13)) by splitting the integral into the $\omega > 0$ and $\omega < 0$ parts, and then making use of the relations $N(\omega) + N(-\omega) = -1$ and $\varepsilon(q,\omega) = \varepsilon^*(q,\omega)$; this leads to

$$\left(\frac{dE}{dt}\right)_0 = \int_{\omega>0} d^3q N(\omega) f(\vec{q},\omega),$$

$$- \int_{\omega>0} \left[d^3q N(\omega) + 1\right] f(\vec{q},\omega).$$

The two terms in $N(\omega)$ cancel exactly, with the result for the stopping power S,

$$S \equiv -\frac{dE}{dx} \cong \frac{-1}{v_p}\left(\frac{dE}{dt}\right)_0 \qquad (15)$$

$$= \frac{2}{\pi}\left(\frac{Z_p e}{v_p}\right)^2 \int_0^\infty \frac{dq}{q} \int_0^{qv_p} d\omega\, \omega \operatorname{Im}\left(\frac{-1}{\varepsilon(q,\omega)}\right)$$

for a projectile ion with inflight charge Z_p.

The only temperature dependence is now contained in the energy loss function $\operatorname{Im}[-1/\varepsilon(q,\omega)]$, and arises from a thermal redistribution of the oscillator strengths in the medium. One can interpret this result as a cancellation between the processes of *stimulated absorption and stimulated emission* of energy $\hbar\omega$ by the projectile, since both processes are proportional to the Planck distribution $N(\omega)$ that characterizes the thermal equilibrium of excitation quanta in the medium. Thus, the energy-loss rate is only determined by *spontaneous emission* processes, which are independent of $N(\omega)$.

3.4. General Trends (Table 1)

As this point, we have to make clear a few obvious assumptions [18].

On most part of their range, the incoming ions are more energetic than the target particles. So, their trajectory may be taken as linear, in view of the very small energy exchange at each encounter. The projectile ions are supposed to be pointlike with a constant charge.

Moreover the usual Z_p^2-dependence of the stopping formula, yields the well-known scaling relation

$$\frac{dE'}{dx}\left(Z_p', M', E'\right) = \frac{Z_p'^2}{Z_p^2}\frac{dE}{dx}\left(Z_p, M, \frac{M}{M'}, E'\right) \tag{16}$$

so we can restrict to protons in the sequel as long as Z_p is kept fixed..

It should be appreciated that one of the main outputs of the present work is the possibility to compute S and Ω^2 for any velocities ratio V_p / V_{th}, because the partial degeneracy is treated exactly.

Thus restricting to the electron fluid component of the target, we get for instance the stopping of nonrelativistic ion projectiles under the well-know high v_b-expression (à la Bethe)

$$\frac{dE}{dx} = \frac{4\pi Z_p^2 e^4}{m v_p^2} nL_e(v_p) \tag{17}$$

with a very accurate asymptotic expression for $L_e(v)$ ($\alpha = \mu / k_B T$)

$$L_e(v_p) = \text{Log}\frac{2mv_p^2}{\hbar\omega_p} - \frac{T_e}{\left(\frac{v_p}{v_F}\right)^2}\frac{F_{3/2}(\alpha)}{F_{1/2}(\alpha)} \tag{18}$$

$$-\frac{T_e^2}{2\left(\frac{v_p}{v_F}\right)^4}\frac{F_{5/2}(\alpha)}{F_{1/2}(\alpha)}, \text{ with } T_e = \frac{T}{T_F} \text{ and } F_s(\alpha) = \int_0^\infty \frac{dx\,x^s}{e^{x-\alpha}+1}.$$

valid at any T_e, which has the two characteristic limits

• **$T_e \ll 1$**

$$L_e(v_p) = \text{Log}\frac{2mv_p^2}{\hbar\omega_p} - \frac{3}{5}\left(\frac{v_F^2}{v_p^2}\right) - \frac{3}{14}\left(\frac{v_F^4}{v_p^4}\right) \text{ (Lindhard)} \tag{19a}$$

• **$T_e \gg 1$**

$$L_e(v_p) = \text{Log}\frac{2mv_p^2}{\hbar\omega_p} - \frac{3}{2}\left(\frac{v_{th}^2}{v_p^2}\right) - \frac{15}{8}\left(\frac{v_{th}^4}{v_p^4}\right)\left(v_{th}^2 = \frac{2k_B T}{m_e}\right) \tag{19b}$$

The energy losses (Fig. **2**) may then be given for any projectile velocity. The T_e-dependence is mostly significant for $E \le 5$ MeV/a.m.u.

3.5. Enhanced Plasma Stopping (EPS)

A lot of theoretical and numerical investigations have already anticipated the presently ongoing experimental programs.

The corresponding argument runs essentially as follows: the standard theoretical framework initially designed for cold matter stopping may be extended to plasma stopping provided due attention is paid to the projectile effective charge as well as to the increasingly significant free electron contribution with respect to the projectile energy loss. More

specifically, these free electrons display an enhanced capability to respond to the incoming electric field. In addition, highly excited bound electrons to the target are also more versatile, and as a result more efficient at taking out the projectile kinetic energy when compared to the least excited ones. These considerations hold as long as the projectile-target electron interaction may be worked out within a Born approximation.
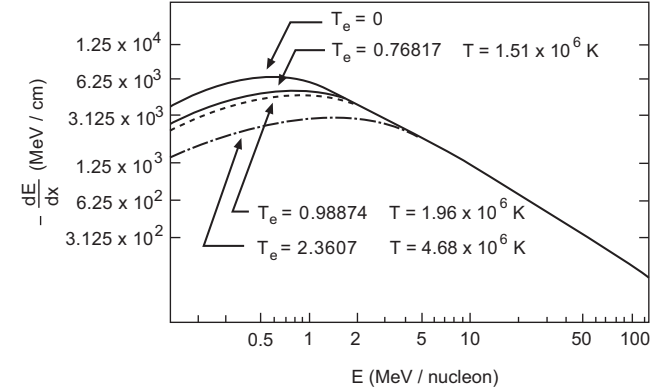

Fig. (2). Free electrons stopping power at n = 10^{25} e-cm^{-3} and several temperatures in terms of the projectiles energy (Ref. [10]).

As a result the theoretical task thus essentially consists of supplementing the above picture with adequate quantitative insight for every projectile-plasma pair of practical interest.

The significant feature of the relevant physics is afforded by the markedly enhanced projectile charge state within the target plasma as compared to its cold target homologue. According to an argument going back to J.S. Bell [19], it is much more difficult for the incoming projectile to get recombined from free electron plane wave states than from orbitals already bound to other target ions. Actually, the respective rates differ at least by three orders of magnitude.

Such an emphasis on a proeminent free electron stopping combined with the enhanced projectile charge leads to expect an enhanced plasma stopping (EPS) compared to cold matter stopping with same electron density in the equivalent target.

The predicted EPS arises from a few simple changes, entirely included in the most straightforward extension to a plasma target, of the well known (Bethe) cold-matter stopping expression. For partially ionized material, free electrons, bound electrons, and plasma ions contribute to energy loss. Ignoring relativistic corrections and the usually very small ion contribution, the stopping power dE/dx is given a standard form as

$$-\frac{dE}{dx} = \frac{4\pi N_0 e^4 \rho}{A_T m_e V_p^2} Z_{eff}^2\left[\bar{Z}\ell n\Lambda_F + (Z_T - \bar{Z})\ell n\Lambda_B\right], \tag{20}$$

where $E = M V_p^2/2$, ρ is the mass density of the stopping medium, N_0 is Avogadro's number, e is the electron charge, m_e is the electron mass, Z_{eff} is the v_p-dependent effective charge of beam ions, A_T is the target atomic weight, Z_T is the target atomic number, $\bar{Z}$ is the average ionization in target, and Λ_B, Λ_F are the arguments of the Coulomb logarithms for bound and free electrons, respectively.

For high target-electron velocities, Λ_B is given by the familiar Bethe expression

$$\Lambda_B = \frac{2m_e v_p^2}{I_{av}}, \qquad (21a)$$

where I_{av} is a geometric average of the effective excitation and ionization potential of the bound electrons. The expression for Λ_F is

$$\Lambda_F = \frac{2m_e v_p^2}{\hbar\omega_p}, \qquad (21b)$$

where ω_p is the plasma frequency. At low velocity, when one has $\Lambda_F < 1$, it must be modified of course.

This expression implies the neglect of any collective stopping effect due to the high intensity of the ion beam, in agreement with recent investigations of the target corona instabilities [20]. It is the high-temperature limit of more sophisticated estimates for the bound- and free-electron stopping power in the dense target plasma. Moreover, for partially stripped projectiles, an equally significant enhanced stopping also arises from the strongly reduced recombination [19], between incoming ion and free electrons. Such drastic behavior maintains a relatively high Z_{eff}, in contrast to that in cold matter, where the ion projectile can easily pick up bound electrons from target atoms (or ions) located near its trajectory. Thus the EPS physical content rests essentially on the much enhanced response of plasma free electrons, together with highly increased Z_{eff} values compared to nominally equivalent cold target, i.e., ones with the same

line-integrated electron density $n_e\ell$ (number/cm^2). n_e is the free-electron density target and ℓ the linear ion range within.

As far as experimental verification of these predictions is concerned, target ionization looks like a much more significant parameter than temperature [18].

Bethe-like stopping appears two or three times bigger in a fully ionized plasma than in the equivalent cold gas with the same density of electrons bound to atomic and molecular orbitals.

Even more dramatic illustrations are shown in Fig. (**3**), where we systematically compare for C^{n+} and U^{n+} the respective evolutions in cold gas and fully ionized hydrogen of Z_{eff} (left vertical axis) and energy loss (right vertical axis) in terms of penetration depth. A Monte Carlo code, making use of every excitation, ionization and recombination cross section, has been developed [21], together with a stopping calculation based on Eq. (20) and Z_{eff} in terms of projectile velocity V_p. Obvious and dramatically different behaviors appear by comparing plasma to equivalent (same linear density) cold-gas results. In both cases, one witnesses striking similarities. In cold gas, Z_{eff} data in terms of penetration range, and pertaining to several ionization stages, decay monotonically from initial value to a common cold-gas asymptotic limit [22] (Z_1 = projectile atomic number)

$$Z_{eff} = Z_1\left(1 - 1.034\exp\left\{-\left[V_p/(2.19\times10^8\,\text{cm}/\text{s})\right]Z_1^{-0.688}\right\}\right) \equiv Z_p, \quad (22)$$

In contradistinction, plasma Z_{eff} rise steadily. For the lightest carbon element, all ionization stages end up in C^{6+} for a maximum range corresponding to the experimental
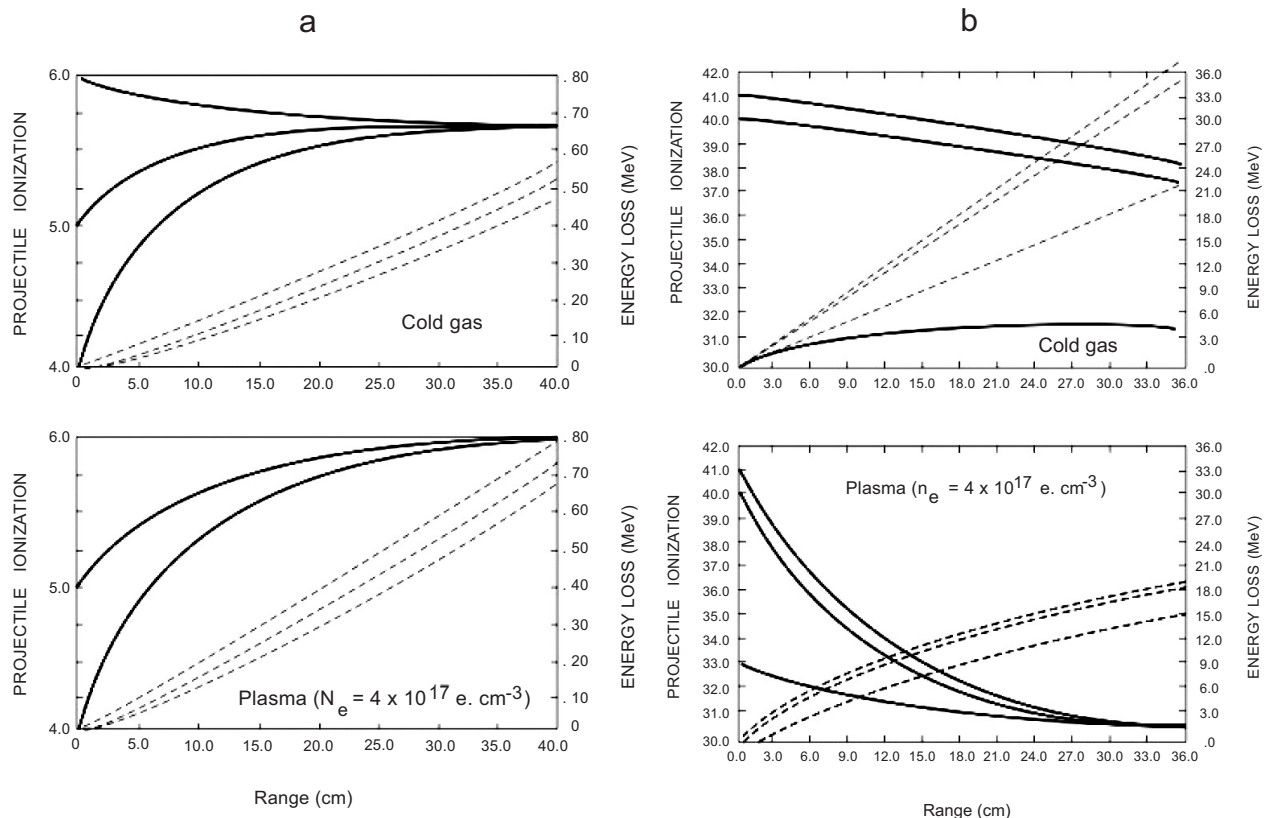

Fig. (3). (**a**) C^{n+} and (**b**) U^{n+} ions at 1.4 MeV/nucleon in cold H$_2$ and fully ionized (2 eV) hydrogen targets (Ref. [21]).

SPQR2 setup detailed below. This effect increases with Z_1. As a rule, projectile effective charges in plasma lie much higher [23] than their cold-gas homologous, except very near the end range, where a kind of catastrophic recombination takes place. As a consequence, stopping powers $\sim Z_{eff}^2$ may increase by orders of magnitude. These specific Z_{eff} behaviors in plasma are essentially due to a quasihindered recombination between ion projectile and target electron. The latter displays a plane-wave behavior that prevents it from being used as a bound orbital. In cold gas, all electron states are bound ones.

Therefore, projectile recombination is made possible by transferring to it a bound electron instead of a target ion. As far as experimental verification of these predictions is concerned, target ionization looks like a much more significant parameter than temperature. We thus expect witnessing these Z_{eff} plasma behaviors, even at a rather modest target temperature, a few eV, provided the target remains fully ionized.

3.6. Non Linear Correction

Within the SSM framework outlined above, (for a fixed $Z_p \equiv Z_{eff}$), it is now straightforward to complete the stopping expression with Barkas $\sim Z_p^3$ and Bloch terms as well. In cold gas, those latter are no longer negligible when the Born parameter $Z_p V_0 / (V_p^2 + V_{th}^2)^{1/2}$ becomes comparable to 1. $V_0 = 1$ in atomic units. V_{th} is the thermal velocity of plasma electrons. Retaining also the very small target-ion contribution, one thus gets a more accurate stopping expression [24]

$$
\overbrace{\phantom{-\frac{dE}{dx}}}^{\text{SSM}}
$$

$$
-\frac{dE}{dx} = \frac{4\pi N_0 e^4 \rho Z_p^2}{A_T m_e V_p^2} Z_T \left[\frac{\bar{Z}}{Z_T} L_0^F + \frac{Z_T - \bar{Z}}{Z_T} L_0^{\bar{B}} + Z_p \frac{V_0}{V_p} \right.
$$

(overbrace label: Barkas)

(23)

Bloch

$$
\left. + Z_p^2 \frac{V_0^2}{V_p^2} f(V_1^2) + \frac{m_e}{A_T} Z_T L_p \right],
$$

↓

Ions

with

$$
L_0^F = Ln \frac{2 m_e V_p^2}{\hbar \omega_p} - \frac{\langle V_{th}^2 \rangle}{V_p^2} - \frac{\langle V_{th}^4 \rangle}{2 V_p^4},
$$
(24)

and $\omega_p = \sqrt{4\pi e^2 n_e / m_e}$, the plasma frequency of the target free electrons.

According to Table **2**, Bethe-like stopping appears two or three times bigger in a fully ionized plasma than in the equivalent cold gas with the same density of electrons bound to atomic and molecular orbitals.

$\langle V_{th}^2 \rangle$ is the usual average in terms of Fermi functions. $f(V_p^2)$ accounts for the standard Bloch correction, which bridges a gap between Bohr semiclassical expression and Bethe quantum-mechanical one. The last term $(m_e/A_T) Z_T L_p$ accounts for inelastic encounters between ion projectiles and target ions. It is nonnegligible only for $V_p \leq V_{th}$, or at very high plasma temperature.

The third term within brackets in the right-hand side (rhs) of Eq. (23) is the Barkas contribution $\sim Z_p^3$. It pertains only to bound electrons and thus vanishes identically in a fully ionized target. In this case, the Born parameter becomes $Z_p V_0 / V_p$.

For $V_p \gg V_{th}$, $L_Q^F \to \Lambda_F$ and $L_0^{\bar{B}} \to \Lambda_B$. The relative importance of the four last terms in the rhs of Eq. (23) is evaluated in Table **2** for a target electron density of subsequent experimental interest. Obviously, the Barkas and Bloch corrections to the main Bethe contribution remain rather weak for all values of the Born parameter $Z_p V_0 / Vp$.

In the sequel Eq. (23) will be often referred to in the canonical form

$$
-\frac{dE}{dx} = k \frac{Z_p^2}{V_p^2} \left[L_0 + Z_p L_1 + f(Z_p^2) \right],
$$
(25)

where L_0 denotes the previous Born random phase approximation (BRPA) contribution, $Z_p L_1$ is the Born II correction equivalent to a Barkas term.

Aside from details associated with physical processes of only secondary importance (residual target ion stopping…), the most crucial assumptions are those involving the validity of the Born approximation and of a classical description. It is these features which cause the main differences between the Bohr, Bethe, and Bloch formulas.

4. ION BEAM-PLASMA EXPERIMENTS: TARGET FIRING

4.1. Parameter Range

The SSM conditions imply $V_p \gg V_{th}$ with

$$
V_p (cm/n\,sec) = 1.38 \sqrt{E/M(MeV/amu)}
$$
(26)

and

$$
V_{th}(cm/n\,sec) = 0.042 \sqrt{k_B T(eV)}
$$
(27)

For a standard target temperature ~ 4 eV, $V_{th} \sim 0.084$, while projectiles with a typical MeV/nucleon energy have $V_p \sim 2$ cm/nsec. Therefore, $V_p \gg V_{th}$ is easily fulfilled. One also easily checks that the ion-ion intrabeam distance remains on average much superior to the electron screening length in the target.

Let us pick up ion beam conditions considered below, with an intensity $I_0 = 500$ nA pulsed with a frequency $\nu = 1.25$ MHz (i.e., a pulse every 800 nsec). The number N_0 of ions within a micropulse is thus

Table 2.   Relative Importance of Bloch and Barkas Terms for Cold-Gas and Plasma Target. The Target has a Linear Density of Free Electron $n_e \ell = 1.5 \times 10^{19}$ cm^{-2} [D. Gardès, G. Maynard *et al.*, *Phys. Rev.* 146, 5101 (1992)]

Ion	E (MeV/amu)	$\frac{Z_p V_0}{V_p}$		Bethe L_0		Barkas		Bloch	
		Gas	Plasmas	Gas	Plasmas	Gas	Plasmas	Gas	Plasmas
C^{4+}	2	0.56	0.62	5.63	12.48	0.08	0	-0.3	-0.35
S^{7+}	1	1.75	2.07	4.94	11.79	0.35	0	-1.16	-1.32
	1.5	1.43	1.69	5.34	12.2	0.23	0	-0.98	-1.13
	2	1.24	1.47	5.63	12.48	0.18	0	-0.85	-1.00
Br^{6+}	0.93	2.79	3.45	4.86	11.72	0.64	0	-1.61	-1.82

$$N_0 = \frac{I_0}{v e Z_{eff}} = 2.5 \times 10^{12} \frac{I_0}{Z_{eff}} \qquad \text{ion/pulse.} \qquad (28)$$

For a typical sulfur ion S^{7+}, this yields $N_0 = 1.8 \times 10^5$ ions/pulse. A micropulse lasts for $\tau = 2$ nsec. With a beam energy E = 64 MeV, the projectile ion's density is $n_0 \cong 10^6$-10^7 cm^{-3}, in a volume containing pulse particles. The interprojectile distance $d_0 = (4\pi n_0/3)^{-1/3}$ gives $d_0 \sim 1.3 \times 10^6$-6×10^5 Å much larger than the target classical screening length λ_D (cm) $= 743$ $(T_e$ (eV)$)^{1/2}$ $n_e^{-1/2}$ (cm^{-3}). For a plasma temperature ≥ 2 eV and Fermi energy

$$\varepsilon_F = 1.84 \left[\frac{4\pi n_e}{3} \right]^{2/3} a_0^2 < 2 \times 10^{-4} \text{ eV}$$

the condition $k_b T_e \gg \varepsilon_F$ is well fulfilled. a_0 denotes the Bohr radius. The corresponding and practically achievable λ_D values ($T_e \cong$ few eV, $n_{e \leq 10^{20}}$ cm^{-3}) are at least three orders of magnitude below the considered d_0 values. Consequently the reduction principle is fully justified in this case. In order to validate the present SSM benchmark, we need a strongly ionized target. The simplest one is hydrogen. The corresponding Saha distribution of protons n_i and atoms n_n is written as (T_e in eV)

$$\frac{n_i}{n_n} = 2.4 \times 10^{21} \frac{T_e^{3/2}}{n_e} e^{-U_i/T_e}, \qquad (29)$$

in terms of ionization energy U_i (eV) and n in cm^{-3}. Above 2 eV, ionization is larger than 90%. The remaining hydrogen bound states are also in thermal equilibrium with free ones, which justifies, *a posteriori*, using the Saha distribution.

4.2. Beam-Plasma Energy Transfer

To secure meaningful energy-loss measurements, one should request that ion stopping does not perturb the plasma thermodynamics. To check up on this point, we compare the expected projectile energy losses to the energy content in the plasma target, We show the beam-plasma energy transfer is indeed negligible. The argument runs as follows.

According to above calculations, one expects that the considered ion beam, with an average width of ~ 0.3 cm, loses 10% of its kinetic energy in a plasma volume $\pi (0.15)^2$ 40 cm^3. This results in a overall 36 μJ energy loss in 2.83 cm^3. Those estimates pertain to the setup detailed below,

which can accommodate 100 ion micropulses for one plasma shot.

Selecting routine plasma parameters, i.e., $n_e = 5 \times 10^{17}$ cm^{-3}, $T_e = 20000$ K, one gets

$$\frac{3}{2}(n_e + n_i)k_B T_e = (1.5 \times 10^{18})(1.73)(1.6 \times 10^{-19}) \text{ J cm}^{-3}, \quad (30)$$

in a volume V ~ 2.83 cm^3.

The plasma volume interacting with the ion beam thus has a 1.19-J stored energy five orders of magnitude above the projectile energy loss (36 μJ). Moreover, this tiny amount of delivered energy is rapidly thermalized within the target through a very high electron-electron collision frequency,

$$\nu_{ee} = 2.9 \times 10^{-6} \left[n_e (\text{cm}^{-3}) \right] \lambda_{ee} \left[T_e^{-3}(\text{eV}) \right] \text{sec}^{-1}, \qquad (31)$$

with Coulomb logarithm

$$\lambda_{ee} = 23 - \ell n \left[n_e^{1/2}(\text{cm}^{-3})T_e^{-3}(\text{eV}) \right]. \qquad (32)$$

Here, we thus obtain

$$\lambda_{ee} = 3.44 \ , \ \nu_{ee} = 2.2 \times 10^{12} \text{ Hz} \ .$$

4.3. Enhanced Deuteron Stopping in Plasmas

Predictions of enhanced ion stopping powers were first made by Mosher *et al.* in 1977 [25]. In that and subsequent investigations by Nardi, Peleg, Bangerter and Zinanon [26] the bound electron stopping was modeled with the Bethe equation and a separate term used for the free electrons.

By 1982 intense ion beams technology had progressed up to the point of allowing a first experimental test of enhanced ion stopping, using deuterons impinging on hydrocarbon and aluminum foils. At 0.3 TW/cm^2, Young *et al.* [7] succeeded in demonstrating enhanced stopping for 1 MeV deuterons. This experiment used neutron time-of-flight from $D(d,n)^3$He reactions in a sandwich target. The energy of neutrons originating before and after the target yielded the stopping power at peak ion beam power.

The experimental arrangement for ion-stopping measurements is presented in Fig. (**4**). An intense beam of deuterons is produced with a cylindrical pinch-reflex diode operated at a peak voltage of about 1.5 MV. The cathode consists of a 6 cm diameter hollow metallic cylinder. The

anode is a 100 μm thick plastic foil coated with a thin layer of deuterated polyethylene (CD_2). This anode is mounted on a carbon support as shown in Fig. (**4**). An electron beam of several hundred kiloamperes emitted from the cathode reflexes through the anode foil and pinches on the anode axis. The heated anode is converted to a plasma, and ions are directed into the hollow cathode where they are charge and current neutralized by a thin polycarbonate (Kimfol) foil and 1 torr air in the focusing-drift region. For a spherically-contoured anode, the ion beam is focused geometrically to several hundred kA/cm^2 at about 4 cm from the anode. A target located at this focus is converted into a dense plasma by this intense ion beam.
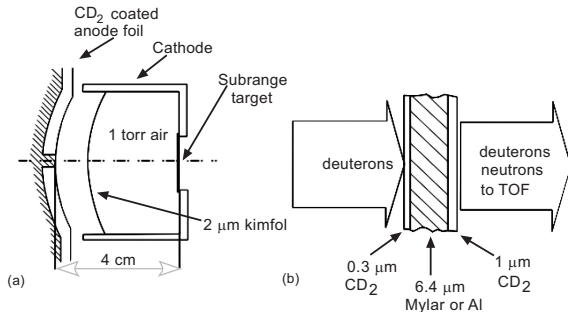
Fig. (4). Schematic (**a**) and target detail (**b**) of enhanced deuteron stopping power experiment at NRL [7].

For ion-stopping measurements, a multi-layered target is used in conjunction with neutral time-of-flight (TOF). The target, as shown in Fig. (**5**) consists of a 0.25 mil thick Mylar or aluminium stopping foil sandwiched between thin layers of CD_2. Measurements of the TOF of neutrons from the two CD_2 targets determines both the incident deuteron energy and the energy loss in the stopping foil on a single shot. Neutrons are detected in the forward direction, and deuteron energies are inferred from measured neutron energies [7].

A significant fraction of free electrons must be produced in the plasma target to alter the ion stopping power. The energy required to create a plasma with significant ionization can be evaluated from equation-of-state tables. Mylar is used in the experiment, and it is assumed that its ionization is similar to that of CH_2. Energy densities approaching a MJ/gm are required to produce an ionization level greater than unity, at least for plastic. By focusing intense ion beams from either planar or curved anodes, the energy densities indicated in Fig. (**5**) have been achieved in the experiments to be discussed

The energy losses measured using planar or spherical diodes and Mylar or aluminium stopping foils are compared in Fig. (**5**) with calculated energy losses for cold targets. The curves are the values expected for cold-target stopping. The measurements are plotted with experimental errors. For planar diodes, horizontal errors arise from a +4 ns
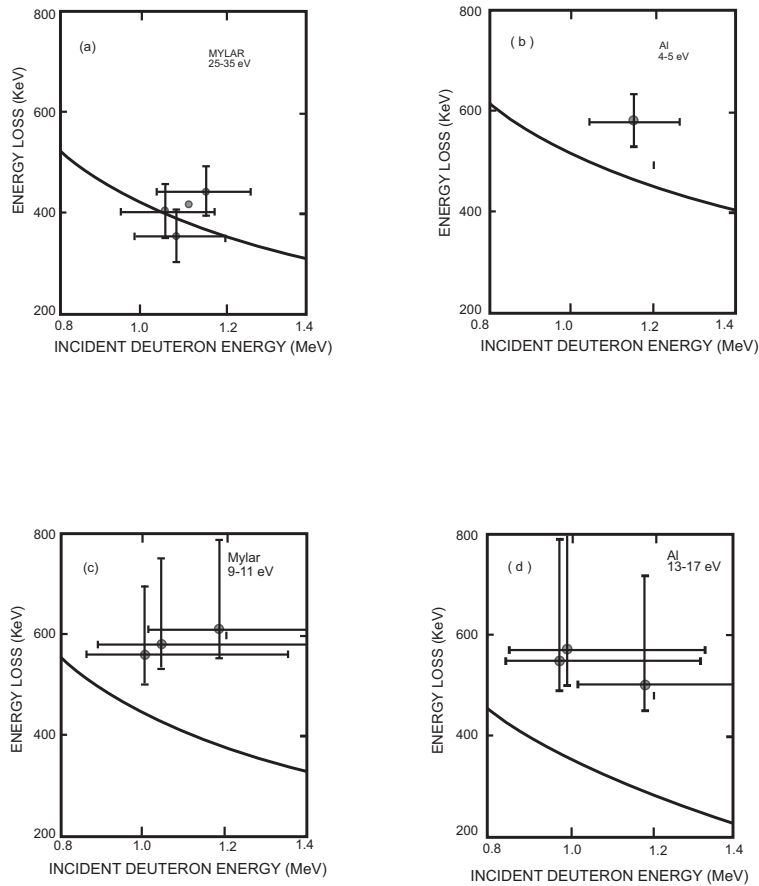

Fig. (5). Comparison of energy-loss measurements for (**a**) and (**b**) planar and (**c**) and (**d**) spherical diodes with energy-loss curves calculated for solid targets. Experimental and computational results; cold target stopping power; NRL experimental results; deposition/hydrosimulation [7].

uncertainty in timing the neutron signal relative to peak ion power. Vertical errors result from + 3 ns uncertainty in the separation of the two neutron peaks. For spherical diodes, errors include uncertainties due to the large range of angles for which deuterons are incident on the target. The measured energy losses are greater than cold-target values, except for the planar diode with a Mylar target. This case is consistent with cold-target stopping.

The measured enhanced ion stopping correlates directly with the degree of ionization expected in these targets.

4.4. Enhanced Alpha Stopping in Hot Aluminum

A related experiment confirming enhanced stopping of alpha particles in heated Aℓ target has been also performed by Toner and his colleagues [27] at the RAL. It makes use of the helium ions produced at 0.75 MeV/amu through imploding a hollow D + T fill with 4 arms of a 6 beam high power laser. The remaining two arms are thus used to produce two hot spots on a thin aluminium foil located within a few millimeters of the imploding target. The salient point is that identical projectiles, i.e. fully stripped He^{2+}, cross simultaneously cold and hot identical material with the same number of scattering electrons. It thus remain to measure the respective stopping efficiency through the corresponding tracks in a CR 39 foil disposed a few mm behind the Aℓ one. One thus observes [27] that Aℓ hot spots (with a central temperature ~ 1 keV) produce a nearly 20% enhanced stopping. However, a detailed and careful investigation of the hot-cold transition on the Aℓ foil is rather involved.

5. ION BEAM-PLASMA EXPERIMENTS: METHODO-LOGY

In order to compensate for the paucity of present days ion beam intensity out of standard accelerators, the SPQR projects foster a simultaneous but independently triggered target firing, synchronized with the ion-plasma interaction out of conveniently bonched ion beam.

This approach has now been pursued in several nuclear physics laboratories for several years. Such experimental activities have thus brought a new brand of plasma physics hardwares in the vicinity of linear accelerating structures: Tandem, Van de Graaf, Alvarez, Linacs… As suggested in Sec. 4, plasma targets are produced either through Z-pinchlike linear plasma columns (LPC) with a 100 µs typical lifetime accomodating many incoming ion bunches or through laser ablated solid surface (LAS) with a much shorter lifetime several tens of nsec, allowing only for one ion bunch through.

Synchronization constraints are obviously much demanding in the latter case. LPC also offer the convenient option of a fully ionized plasma of light elements: hydrogen, deuterium which allows to probe SSM predictions with a high level of confidence by restricting to ion projectiles energy losses with target free electrons and practically no inflight ion recombination. LAS allows for a much larger variety of plasmas: He, Li, C, Al,… wich often remains partially ionized, only. One then expects a rather strong interaction between ion projectile remaining electrons and those bound in the target. Clearly, in that occurrence, the

quantitative implementation of SSM predictions gets more involved. It should then proceed through a tedious evaluation of the velocity dependent ion projectile charge $Z_{eff}(V_p)$.

However, it is also a rewarding feature providing additional opportunities for adjusting ion beam range in the dense plasma target.

5.1. Linear Plasma Column (LPC)

The schematics of the so-called SPQR2 device (Figs. **6**, **7**) developed by Chabot, Gardès *et al.* at IPN Orsay shows how the firing of the LPC (nel ~ 10^{19} e-cm^{-2}, interelectrode distance ~36 cm) can trigger a Tandem accelerator. Ion projectiles exiting the target plasma (TP) are then finely diagnosed in charges and energy through a magnetic split-pole device. Fast valves operating on a msec time scale at boths LPC ends prevent plasma leaking in the pipe vacuum thus securing an accurate evaluation of plasma fluence (linear density) $n_{e\ell}$. Finally the transient plasma parameters (n_e, T_e, …) have to be diagnosed on line, which is not the easiest part of the whole procedure. Toward this goal one often makes use of tiny amounts of desorbed neutral hydrogen atoms to perform optical or spectroscopic diagnostics based on the Stark effect resulting from their interaction with the surrounding plasma. Broadening and shift of corresponding line transitions between excited atomic states then provide detailed information on TP parameters.

The plasma parameter most relevant to the energy-loss measurement is the density of free electrons (n_e), whereas the variation of the electron temperature T_e is of minor influence as long as the ion velocity is large compared to the thermal velocity of the electrons. For the assessment of energy-loss contributions of free electrons relative to the stopping power of bound electrons, which are still present in nonionized hydrogen molecules and atoms, it is necessary to know the degree of ionization. Assuming local thermal equilibrium (LTE) in the plasma these three quantities are, however, strongly related to each other through the Saha equation. Thus with two of these parameters determined experimentally the third one can be calculated.

One can use two different methods for plasma diagnostics: spectroscopy in a side-on spectroscopy and laser absorption measurements along the beam-plasma interaction axis. The plasma is optically thick along the axis for the H_β emission; therefore spectroscopic measurements have to be performed side on. With a system of a spectrometer coupled to a streak camera, one measures the light emission from the plasma resolved in wavelength and in time. The free-electron density n_e is determined from the half-width of the Stark-broadened H_β-line. From intensity ratios of the line radiation to the emission from the continuum the free-electron temperature T_e can be derived. Typical values observed in these experiments are $n_e = 3 \times 10^{17}$ cm^{-3} and $T_e = 2$ eV and occur at maximum energy loss. Evaluation of the Saha equation for these plasma parameters yields an almost fully ionized plasma.

Beam diagnostics (at the percent level) is efficiently provided by noninteractive capacitive probes located at both target ends, followed by a few meters long time-of-flight (TOF). Capacitive probes are parts of an oscillating circuit
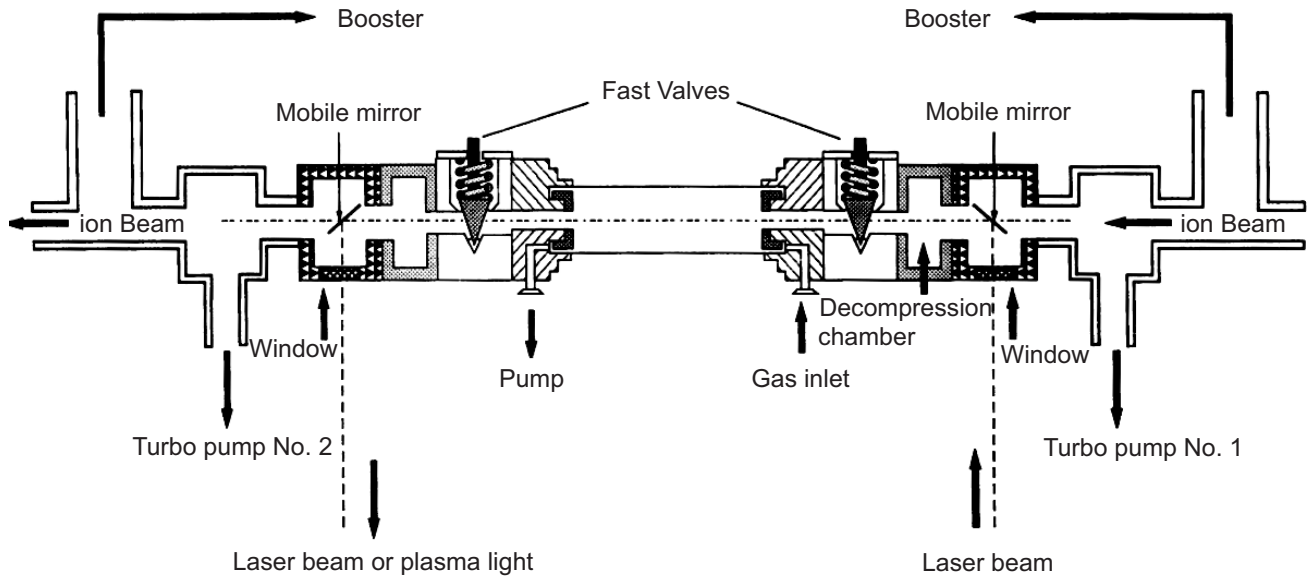
Fig. (6). Experimental setup. A linear plasma coloumn is confined in an alumina tube connected to the beam line with two fast valves. Plasmas diagnostics are realized using a laser beam injected during the plasma shot *via* two removable mirror systems (Gardes *et al.* [21]).
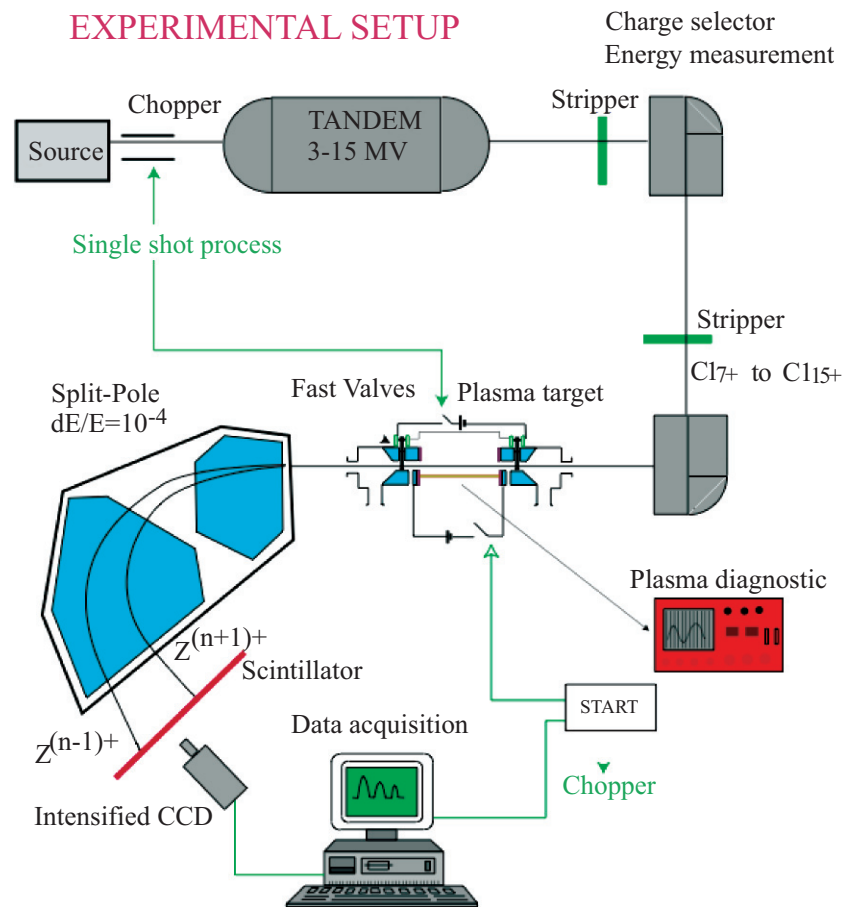

Fig. (7). SPQR2 experimental set-up.

with a varying impedance when the ion beam makes it through them.

As far as SSM-experiment confrontation is concerned, one expects an overall linear n_e-dependence of energy losses ΔE. This is confirmed on Fig. (**8**). for S^{n+} ions at 1 MeV/amu

in deuterium plasma. Time histories of both quantities parallel each other with a good accuracy.

Moreover, the measured energy losses for S^{7+} and B_r^{6+} increase according to SSM predictions with LPC linear

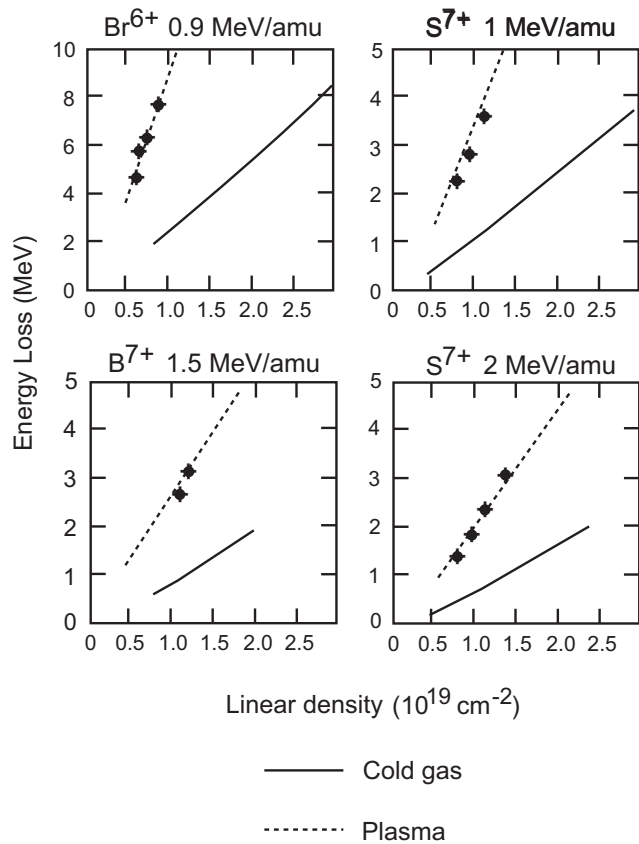density (Fig. **8**). They appear several hundreds per cent bigger in plasma than in equivalent cold gas target.

Fig. (8). Energy losses as a function of free plus bound-electron dentsity in a hydrogen plasma for Br^{6+} with 0.93 MeV/amu and also S^{7+} with 1, 1.5, 2, and 2 MeV/amu, respectively (Gardès *et al.* [21]).

5.2. Laser Ablated Plasma Target (LAPT)

The interaction chamber where bunched ion beam and laser produced plasma meet according to the general scheme given above is depicted on Fig. (**9**) for the so-called SPQR1 project developed at Bruyères-Le-Chatel [28].

This setup allows to emulate more realistically the driven-pellet interaction expected in ion driven inertial fusion. We now consider laser ablation of nonhydrogenic planar targets of low Z materials such as carbon and aluminum. Their low atomic number secures a large proportion of free electrons under light irradiation. Therefore, we expect a large EPS and a large enhanced projectile ionization in plasma (EPIP) as well.

Typically, one envisions plasma parameters such as $1 \leq T_e$ (eV) ≤ 150 and $10^{17} \leq n_e$ (cm^{-3}) $\leq 10^{19}$. A CO$_2$ laser ($\lambda = 10.6$ µm) delivers an irradiance $\sim 10^{11}$ W.cm^{-2}. The target is submitted to a 10^{-7} mbar vacuum. In order to synchronize the laser with the heavy ion beam, one keeps to a minimum the mismatch between plasma production and arrival of ion bunches. So, the laser discharge is ignited with a synchronous signal from the accelerator by another Nd-YAG laser, with weak time fluctuation. The considered setup can deliver a 20 J pulse with a 50 nsec half-maximum duration.
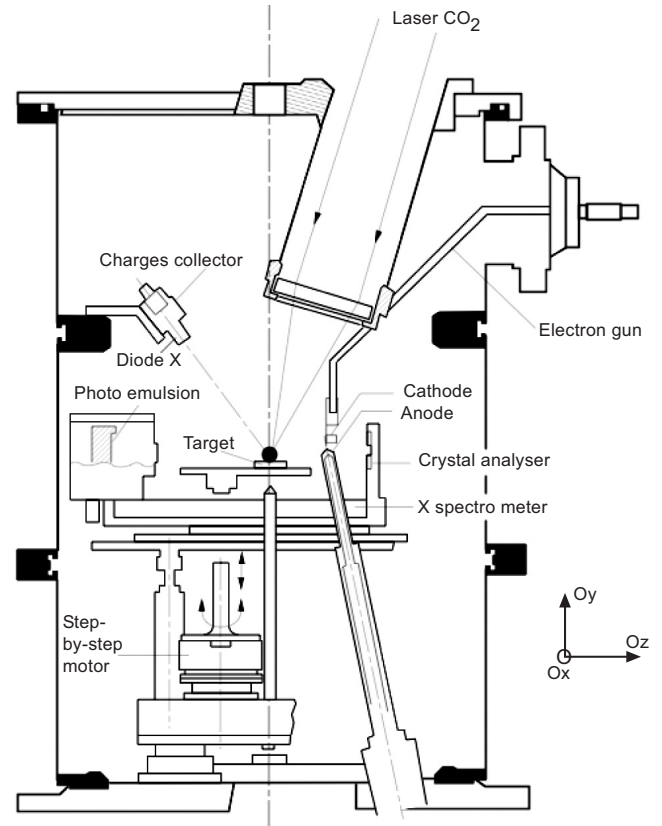

Fig. (9). Interaction chamber. The ion beam propagate along x axis (Couillaud *et al.* [28]).

5.2.1. General

The impact of laser light on target produces an immediate ionization, with a charge density decreasing from the ablated surface. Plasma gets heated within a few picosecondes through inverse bremsstrahlung in a zone thickness comparable to a laser wavelength. The kinetic pressure raises very rapidly, so the plasma starts expanding from the struck place with a velocity close to sound velocity.

Simultaneously, the plasma ablation produces through momentum conservation, a compression wave preceded by a shock wave. The plasma absorbs light as long as its frequency ω_{pe} remains smaller than the laser frequency $\omega_{10.6\mu m} = 1.78 \ 10^{14}$ rad/sec^{-1}. So, the photons do not penetrate a plasma with $n_e \geq n_{ec} = 10^{19}$ e-cm^{-3}. When $\omega \geq \omega_{pe}$ ($n_e \leq n_{ec}$), the laser wave propagates in plasma and gets attenuated. In a Al plasma with $T_e = 100$ eV, $\bar{Z} = 7$, the absorption coefficient is $K = 2.3$ x 10.3m^{-1}. CO$_2$ laser light is then absorbed on a 430 µm thickness.

On the other hand, when $n_e > n_{ec}$, light gets specularly back reflected with a T_e-independent absorption coefficient

$$\kappa = \frac{2\omega p_e}{c} = 3.75 \times 10^{-6} n_e^{1/2} (cm^{-3}), \tag{33}$$

Three-body recombination should remain much smaller than radiative recombination in an optically thin plasma. In order to simplify plasma diagnostics, one is particularly

interested in a stationnary regime. The density of plasma ions with charge Z then fulfills dNz/dt=0, so that

$$\frac{n_{Z+1}}{n_Z} = \frac{S(Z,T_e)}{\alpha(Z+1,T_e)}, \tag{34}$$

in terms of $S(T,T_e)$, ionization coefficient and/or collision, and $\alpha(Z+1,T_e)$, radiative recombination coefficient. The effective ionization time is given by the longest and last ionization, i.e.

$$\tau_Z = \frac{1}{n_e\left[S(Z_{max}-1,T_e)+\alpha(Z_{max},T_e)\right]}, \tag{35}$$

which is close to the heating time when ionization and recombination equilibrate each other, so that

$$S(Z_{max}-1,T_e) \cong \alpha(Z_{max},T_e), \tag{36}$$

which yields $\tau_Z \sim (n_e S)^{-1}$ and

$$\tau_Z(\text{sec}) = \frac{10^{12}}{n_e(\text{cm}^{-3})}, \tag{37}$$

The stationnary plasma assumption allows to connect the ion charge in target to electron temperature through [28] (Z_T = target atomic number)

$$\overline{Z} = 26\left(\frac{T_e(\text{keV})}{1+\left(\frac{26}{Z_T}\right)^2 T_e(\text{keV})}\right)^{1/2}, \tag{38}$$

5.2.2. Charge Distribution at Fixed N_e and T_e

Operating the SPQR1 device enables us to study the interaction of Cu^{q+} ions in the $0.6 \leq \frac{E}{A} \leq 0.8$ MeV a.m.u. energy range, with synchronously fired C and Al plasmas. The corresponding hot targets have an electron temperature $2 \leq T_e$ (eV) ≤ 110, and an electron density $10^{17} \leq n_e \leq 10^{19}$ cm^{-3}. They are typically a few mm thick. The ion beam-plasma interaction takes place at 1 mm (core) and 5 mm (corona) above the cold target plate.

Now, we turn to distributions of projectiles charge states at the exit of C and Al plasmas. Observation of a complete Y_q-distribution is obtained through a series of laser shots with fixed parameters (interaction time, laser power, etc …).

On captions featuring experimental Y_q data, one also superimposes (see Fig. **10**) a Gaussian distribution

$$Y_q = (2\pi d^2)^{-1/2}\exp[-(q-\overline{q})^2/2d^2], \tag{39}$$

with same $\overline{q}$ and d as experimental distribution. Usually $\overline{q}$ is not an integer. However, $\overline{q} = q_{max}$ for symmetric cases.

So, let us first consider a C target with initial temperature T_e = 70 eV and T_{inter} = 5 eV (cf. Fig. (**10**)). Ion beam penetrates dense plasma core at 1 mm above target plate with a time delay Δt=200 nsec. Then, observed Y_q distribution is very close to a gaussian for $q \cong \overline{q}$. Discrepancy slightly increases with $|q - \overline{q}|$.
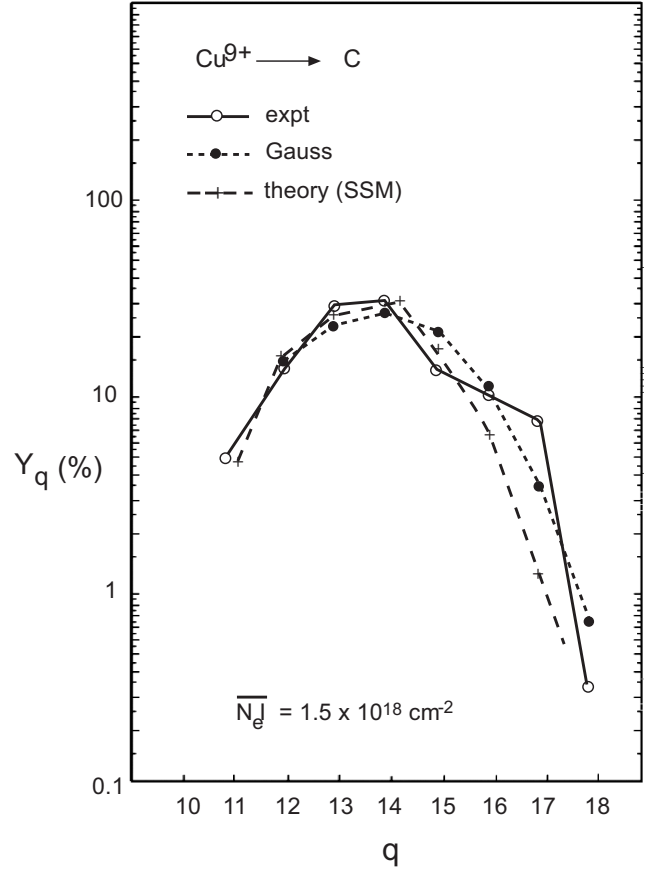

Fig. (10). Y_q-distribution in a C target (Table **3**) with gaussian fit. The SSM theoretical result is obtained for a density $n_C^{5+} = 3*10^{17}$ cm^{-3} (Couillaud *et al.* [28]).

6. HEAVIER ION PROJECTILES

6.1. Hydrogen Plasma Target

The above metrological approach allows for a systematic investigation of the ion-plasma interaction on any linear accelerating structure providing beam bunching. This manipulation can increase up to three orders of magnitude the initial coasting intensity. Heavier ion projectiles with larger Z should experience a Z^2 enhanced stopping (Sec. 3) at high velocity (w.r.t. thermal electron velocity in target

Table 3. Experimental Parameters of the Y_q-Distribution featured on Fig. (10)

Plasma			Heavy ions : $\sum Y_Q = 100$						
T_e	T_{int}	$\overline{n_e\ell}$	$\overline{q}$	q_{max}	$\overline{q^2}$	width d	asymmetry s		$\overline{q_G^2}$
(eV)	(eV)	(cm^{-2})							
			Interaction at 1 mm						
60	60	$1.5.10^{18}$	13.9	14	194.5	1.5	0.31		195.5

especially). This explains that SPQR-like plasma targets have also been installed on the Alvarez section (1.4 MeV/nucleon) of the UNILAC at GSI-Darmstadt which can deliver arbitrarily charged heavy ion beams (see Hoffmann *et al.* [29]) (see Fig. **11**). GSI-LPC slightly differs from Orsay one by a double beam deflection at both of the LPC beam line to allow for on-line plasma diagnostics through laser interferometry of the ignited discharge.
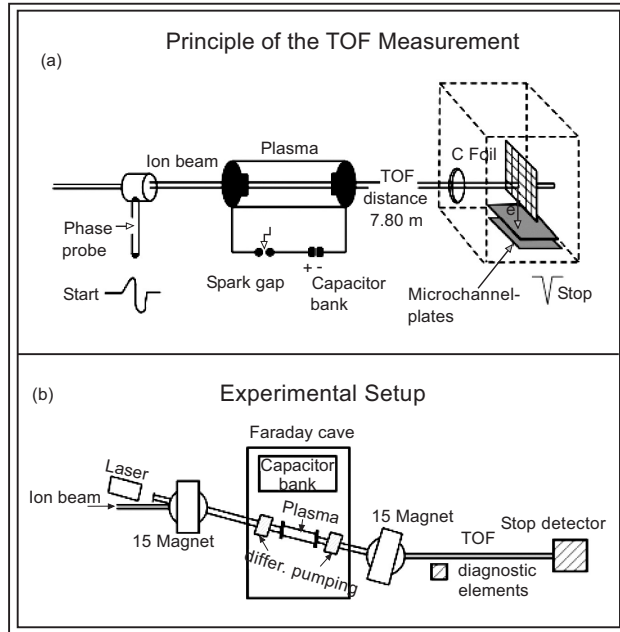

Fig. (11). Schematic setup of the GSI experiment (Hoffmann *et al.* [29]).

A laser-absorption measurement provided a second independent method to diagnose the plasma parameters. The diagnostic measurement in this case is performed along the axis of the plasma column, collinear with the ion beam zone of interaction. The transmitted fraction of the initial intensity I_0 depends strongly on the frequency of the laser light and on the plasma parameters n_e and T_e and can be written as

$$I = I_0 \exp[-\kappa(\lambda, n_e, T_e)\ell],$$

where ℓ is the length of the absorbing layer and κ the absorption coefficient. Hence, when the absorption coefficients of two different wavelengths are known, the parameters ne and T_e can be determined. The two most intense lines of the argon-ion laser, used in this experiment, are $\lambda_1 = 488$ nm (blue) and $\lambda_2 = 514$ nm (green) and coincide nearly with the H_β-line and transitions in the continuum, respectively. The experimental setup to measure the absorption runs as follows. An air-cooled argon-ion laser is used with an adjustable power output between 4 and 400 mW was used. After passage through plasma the beam is split in two components and each subbeam passes through a wavelength filter of 488 and 514 nm, respectively. Lenses focuse the beam components onto optical fibers to transmit the light to photodiodes especially sensitive in this wavelength regime. Photodiode signals is registered on a storage oscilloscope. With this method the transmitted laser-beam intensity can be measured with high time resolution for both wavelengths during one single plasma ignition.

The development of the ion charge state during the passage of the target depends strongly on the target state. Electron-capture processes from bound target electrons will decrease the ion charge state rapidly while it traverses the cold hydrogen gas. In a plasma target, however, electron-capture processes are reduced, since only free electrons are present. Ionization due to collisions with target nuclei is the dominant ionization mechanism and does not change significantly with a rise of temperature in the few-eV regime. Therefore ionisation rates prevail over electron-capture rates and the charge state tends to even increase further while the ion moves through the target. It is an important feature of this experiment that the initial charge state of the ions is always chosen 10-15% above the equilibrium charge state in cold gas. Therefore, even in a comparatively low-density target ($n_e = 10^{17}$ cm^{-3}) the effective charge of the ions starts to develop in opposite directions, depending on whether the target is cold hydrogen gas or a fully ionized plasma.

Given GSI energy loss results displayed on Fig. (**12**) pertain to the Alvarez section of the UNILAC with an initial energy ~1.4 MeV/amu. Theory refers to SSM, which remains secured for those experiments as well as for the IPN Orsay ones. In a typical target plasma with $T_e = 2$ eV,

$n_e = 4 \times 10^{17}$ e-cm^{-3}, the nonlinearity parameter $\frac{Z_{eff}(V_p)}{n_e \lambda_D^3}\left(\frac{V_{th}}{V_o}\right)^3$

~ 0.2 for U^{30+} at Alvarez energy.

As in the above SPQR (Orsay) experiments, one can notice a very significant EPS throughout the periodic table, from Calcium to Uranium.

In this figure only those calculations are shown where the variation of Z_{eff} with increasing target thickness is considered. For all six ion species used in these experiments a significant plasma EPS is observed. The theoretical model is in good agreement with the experimental results. The stopping power increase varies from a factor of 2 for the heavy ion with the smallest mass number (^{40}Ca) to 2.6 for uranium.

6.2. Helium Plasma Target

In contradistinction to the above hydrogen ~deuterium plasma targets which are nearly fully ionized at $T_e = 2$ eV, Helium plasma at 5 eV still retains as many bound electrons as free ones.

Corresponding Z pinch targets have been exposed by Neuner, Ogawa *et al.* [30] to the Ar beam at 6 MeV/amu out the HIMAC facility in Chiba. The given setup is depicted on Fig. (**13a**).

The discharge tube has a dimension of 165 mm × 28 mmϕ. Helium gas flows to the discharge tube with a pressure of 110 Pa. Preionization is triggered with a current of 30 A to achieve a uniform pinch. The preionization is followed by a main discharge of 40 kA at 16 kV driven with a capacitor of 4 μF. Time jitter of the z-pinch discharge is ~10 ns. Discharge currents are supplied by six coaxial cables, which surround symmetrically a z-axis of the tube, to achieve a uniform plasma with axial symmetry.
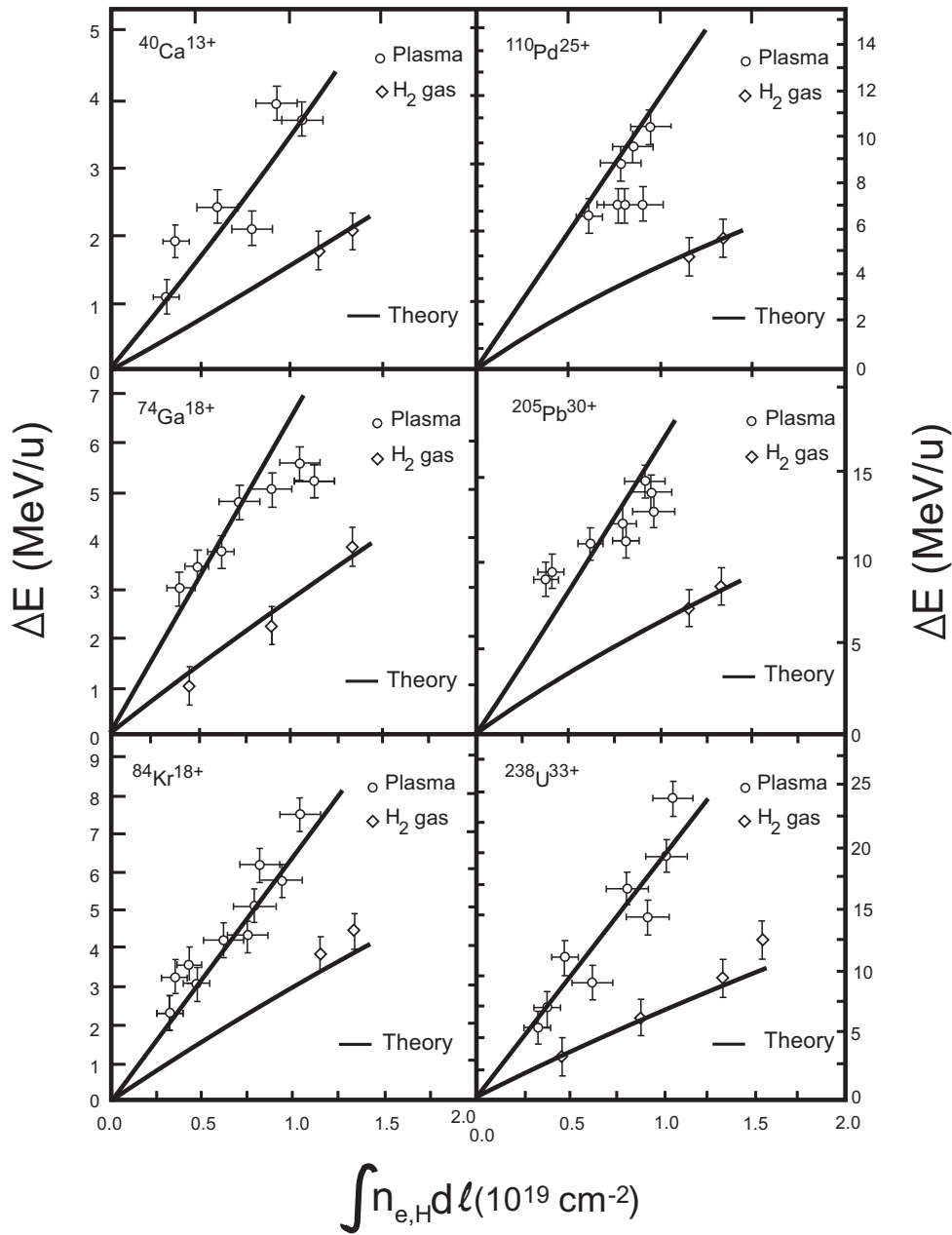
Fig. (12). Energy-loss data (GSI-Darmstadt) and theory for different ion species. 1.4 MeV/a initial energy. Theory refers to SSM.

Main discharge current rises to its maximum 2 μs after discharge starts. The dynamical process of the pinch is examined through pictures with a streak camera. The first pinch occurs at 1 μs when a shock wave reaches the z-axis. The second pinch is formed at 1.7 μs when a current sheet collides with the reflected shock wave.

Stark broadening of the He II 486.6 mm line provides n_e and T_e is derived from suitable lines ratio. A beam of 6 MeV/u Ar^{17+} is injected to the plasma target. The pulsed beam lasts for 10 ns. Time signals of the beam are picked up with a coil as a reference for TOF measurement.

Fig. (**13b**) indicates the time evolution of the degree of ionization and the mean charge state with electron density observed side-on.

Fig. (**13c**) compares the experimental stopping power of the Ar ions in the helium plasma with the theoretical evaluation. Three curves represent the calculation for cold matter and helium plasma with $Z_{eff} = 17$ and 18 respectively. The stopping power measured for the plasma is larger by a factor of 2 to 3 than the cold matter estimate. Plasma effect in the energy loss was observed 1 to 1.8 μs after the discharge starts. The curve for $Z_{eff} = 18$ reproduces the experimental data points for the first pinch.

6.3. Projectile Charges-State Distribution

Operating the Orsay linear tandem accelerator from the SPQR2 discharge tube (see setup on Fig. **7**), it has been possible to proceed to a fine structure investigation of the
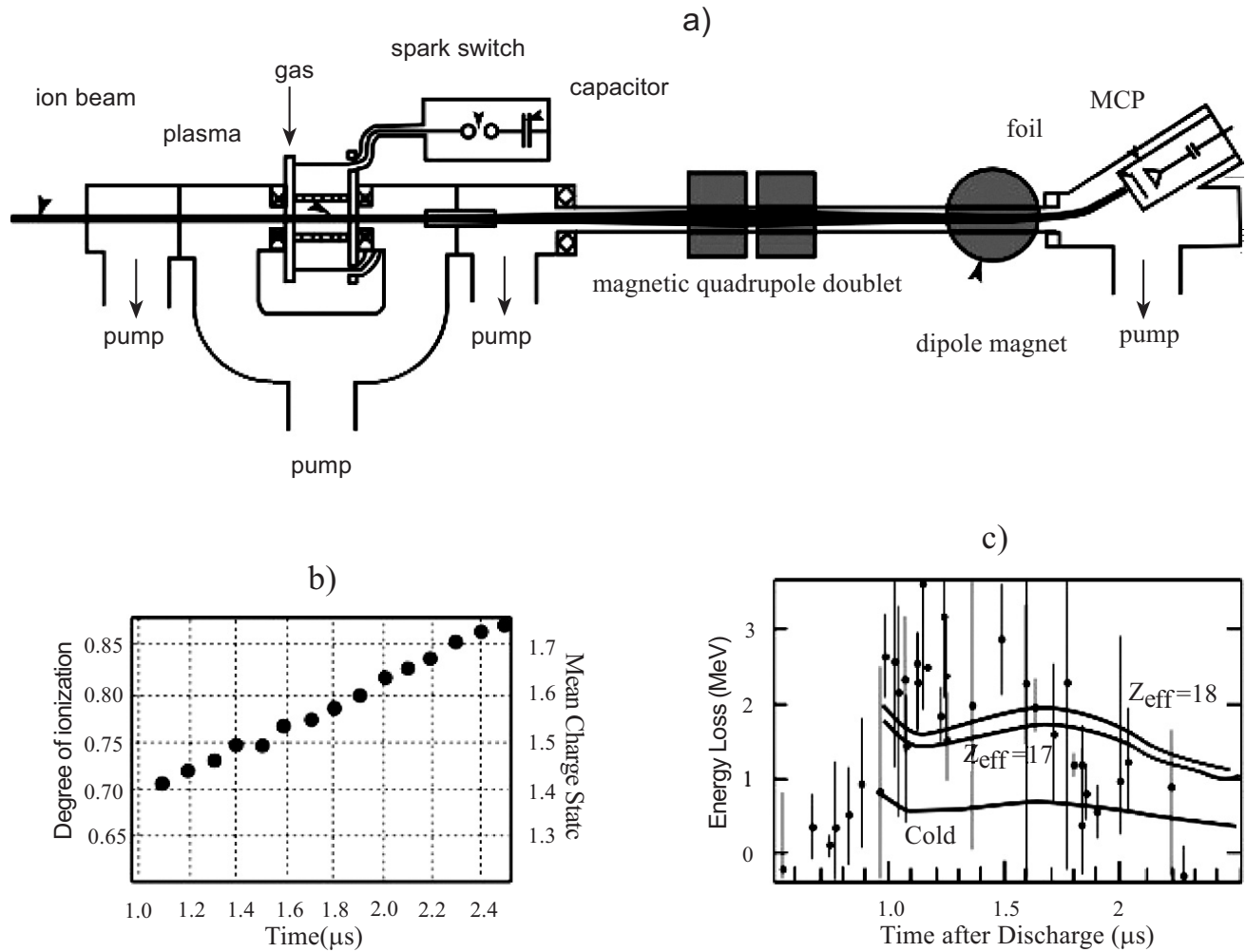
Fig. (13). TIT-HIMAC Z-pinch device and interaction set-up (Neuner *et al.* [30]).

plasma stripping effects on highly charged chlorine ions in the MeV/u energy range [31].

Spectroscopic and optical methods when applied to target plasma are not very sensitive in detecting very small contamination rates of (heavy) impurities. However, such a contamination can strongly affect the evolution of the charge distribution of the chlorine ions relative to situations in pure plasma or cold gas. For this purpose, an ion beam was used as a probe to investigate both heavy element impurities and proton density. The principle of the measurement is based on charge-exchange and ionization processes on a hydrogenlike chlorine ion beam (Cl^{16+}) at 4.3 MeV/u. For this particular beam, it is found that the main contributions for electron capture and ionization come from the heavy contaminants and the protons, respectively. With these conditions, measurements on Cl^{15+} heliumlike ion production and Cl^{17+} bare ion production provide, respectively, access to the heavy element and proton densities inside the plasma target. A good agreement was found with the optical diagnostic presented previously for the proton density and was compatible with the residual pressure (2×10^{-3} torr) measurement for the heavy elements contamination.

After interacting with the plasma target, the ions were analyzed with a magnetic dipole. Localization of impact corresponding to the charge-state distribution and energy loss was done using a fast scintillator (NE102) viewed by a Charge Coupled Device (CCD) camera. Digitized images were stored and visualized in a personal computer. The efficiency of detection was 100%. A typical beam burst of 1 μs width led to some thousands of ions on the scintillator detector.

The data were analyzed using the Physics Analysis Workstation (PAW) software CERN library.

For the two incident charge states 13^+ and 15^+, the final charge-state distributions after interaction with fully ionized hydrogen are compared in Fig. (**14a**, **b**) to the corresponding cold-gas distributions. This comparison has been performed during the optimum transmission period. At that moment the linear-density of the target was $(1.0 \pm 0.1) \times 10^{19}$ e$^-$/cm^2 with $95 \pm 5\%$ ionization degree. The enhancement of the stripping efficiency of the plasma medium shows up clearly with the 13^+ incident projectile. The mean charge state is displaced from 13.18 up to 13.87 in the plasma case. For the 15^+ incident charge (Fig. **14b**), a frozen charge-state effect is observed, in agreement with channeling experiments [31].
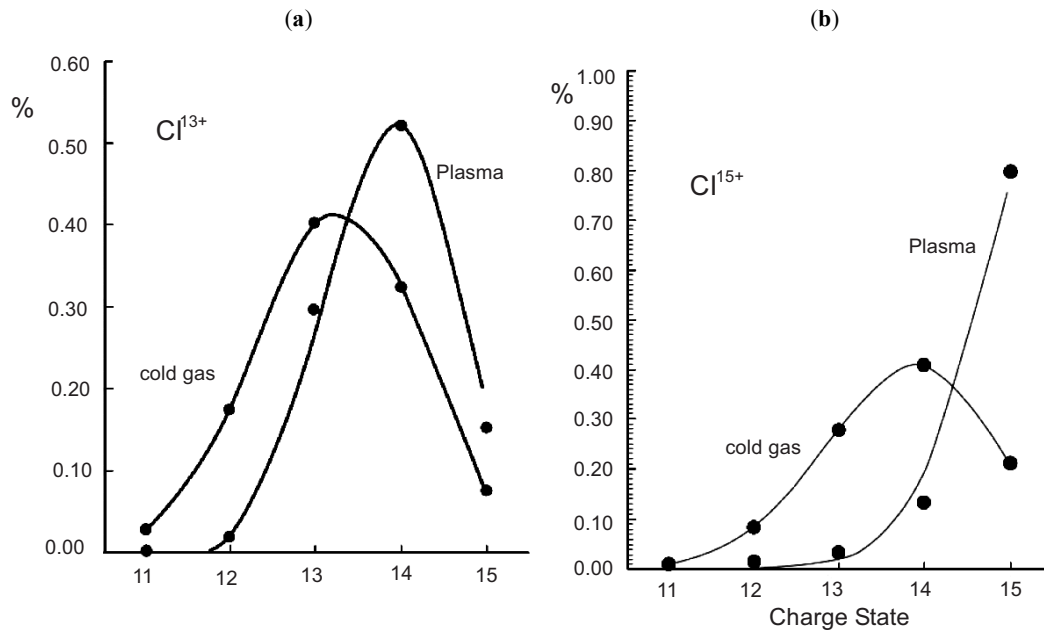
Fig. (14). Comparison between cold-gas and plasma charge-state distribution. The lines represent the model calculation for cold gas (dashed line) and plasma (solid (**a**) Cl^{13+} incident ion; (**b**) Cl^{15} incident ion) (Chabot *et al.* [31]).

The error bars that are reported on the graphs reflect experimental uncertainties on peak localization, gaussian fitting, and remaining plasma lens effects.

A modeling solving rate equations for the various and final ion charge states is compared to experimental results for charge-state distribution in cold gas and plasma.

The calculation in the Plasma case is based on the following three assumptions (see Sec. 3).

(i)   The capture cross section of free electrons is zero. This approximation is justified considering that the cross sections associated with radiative charge transfer are roughly three orders of magnitude lower than the bound-electron capture cross sections. Moreover, dielectronic recombination processes are determined by resonant features that need not be considered in this particular velocity range.

(ii)   The ionization cross section for the free electron-proton pair is taken to be half the ionization cross section for the hydrogen molecule. That is to say that the proton is not screened by the bound electron and that ionization by bound or free electrons is equal.

(iii)   The cross sections on the impurities are the same in the cold gas and in the plasma medium.

The plasma temperature (2 eV) is not high enough to ionize more than one outer shell electron of heavy impurities. This electron makes only a small contribution to the total charge transfer cross section and its role in the screening remains negligible for the ionization process.

Fig. (**15**) clearly demonstrates the charge changing behavior due to the plasma target: an unchanged ionization and a strongly reduced capture. In the plasma case the residual capture arises only from the remaining neutral hydrogen (some percent of the total density) and also from the heavy impurities. The crossing between the ionization

and the capture curves correspond to the equilibrium charge values.

In the general case of ion interaction with matter, three media can be distinguished for charge changing:

(i)   The cold-gas medium where all the ionization and capture processes are effective.

(ii)   The free electron medium, like that in channeling experiments, where then main capture and ionization processes are suppressed (no more ionization by nuclei).

(iii)   The plasma medium where capture is reduced, like in channeling experiments, but where ionization on nuclei remains significant.

As a consequence, the plasma target appears as the most effective stripping medium for heavy ion beams in the MeV/u velocity range.

7. LOW VELOCITY ION STOPPING

If one had to express in one diagram, the basic features of the SSM stopping model one is likely to come up with that one depicted on Fig. (**16**) which advocates maximum projectile stopping at $V_p \geq V_{the}$. V_{orbit} designates bound electron velocity in target. Corresponding indications have been successfully confirmed experimentally.

7.1. Krypton in Hydrogen

Much slower heavy ions with a few tens of keV/nucleon are then expected to exhibit a very high EPS value in a fully ionized SPQ2-type hydrogen discharge. For instance, Jacoby and his colleagues [33] have used a radio-frequency-quadrupole (RFQ) linear accelerating structure, the socalled Maxilac (Fig. **17**) at GSI to investigate the stopping power at low beam energies of singly charged Kr^+ ions at 45 keV/u (38 MeV).
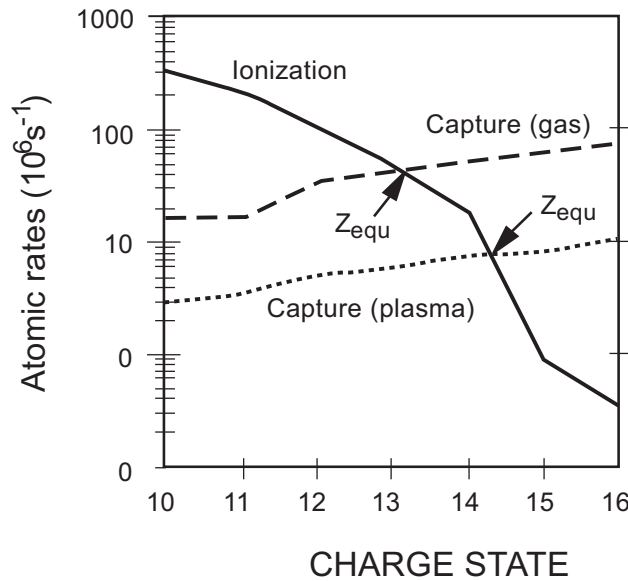
Fig. (15). Ionization and one electron capture rates versus the projectile charge state for Cl^{q+} at 1.5 MeV/u in gas and plasma target, respectively (Maynard *et al.*, [32]).
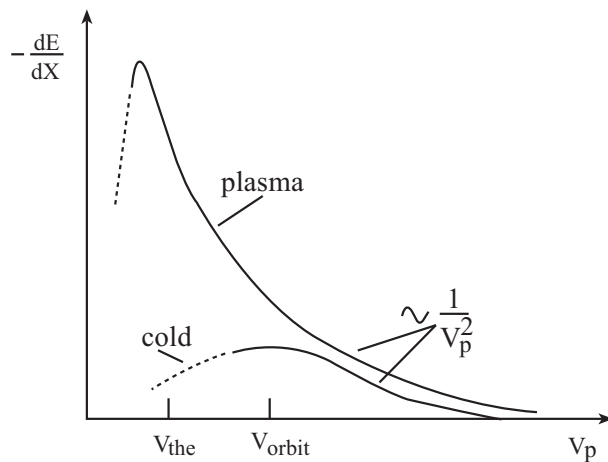

Fig. (16). Schematic drawing of the stopping power dE/dx as a function of projectile velocity for cold gaseous targets and plasma target. The same constant Z_{eff} is assumed in both cases.

However, the initial ion velocity is ten times as high as the target electron thermal velocity, so that the Bethelike formulation of the SSM still makes sense.

7.1.1. Experimental

A homogeneous plasma is produced in a 20 cm long cylindrical quartz tube. A capacitor bank (2.6 μF, 5-10 kV) supplies discharge currents of 10-20 kA to the plasma. This current is oscillating with a half period of about 4 μs. At initial hydrogen gas pressures of 0.5-2mbar, electron densities of up to 10^{17} cm^{-3} are produced in the discharge. The two-stage differential pumping system consists of a powerful root pump and two turbomolecular pumps at the second pumping stage, each reducing the pressure by about a factor of 100. Discharge tube, root pumping, and turbomolecular pumping are separated by small apertures (diameter of 3 mm, length of 30 mm), which allow a windowless penetration of the ion beam into the plasma.

These small apertures define the beam path through the plasma close to the optical axis of the discharge tube.

7.1.2. Results

A comparison of the measured stopping power of plasma and of cold hydrogen gas with theoretical calculations is shown in Fig. (**17b**). The solid lines represent theoretical calculations of the hydrogen plasma stopping power performed with a Monte Carlo code based on charge transfer cross sections. Theoretical values for the stopping power of cold hydrogen gas are represented by the dash-dotted line. For cold hydrogen gas the experimental result yields 33 ± 5 MeV/(mg/cm^2). The dashed area represents the region of stopping power achieved with the maximum charge state expected for a fully ionized plasma (upper curve) and the stopping in a plasma obtained with charge states of cold hydrogen gas (lower curve). The Monte Carlo simulations indicate that, for the energy regime of this experiment, a fraction of a few percent of the used plasma length is sufficient to obtain the calculated charge states. For an average ion energy of about 40 keV/u, a hydrogen plasma stopping power of 1080 ± 210 MeV/(mg/cm^2) is measured. The experimental value at 1.4 MeV/u was obtained during an earlier plasma stopping experiment performed at the UNILAC accelerator [29].

Given the energy of 45 keV/u, an effective charge state of about $Z_{eff} = 2$ is calculated for krypton in cold hydrogen gas. Comparing the rates for ionization and recombination in the plasma (taking into account dielectronic recombination and inverse photoeffect) effective charge states $Z_{eff} = 3.1$, 4.5, 6.4, and 7.8 are expected for an ionization degree of 90%, 99%, 99.9%, and 100%, respectively. Because the recombination rate in cold gas is 2 orders of magnitude larger than the recombination rate in a fully ionized plasma, even small contributions of cold gas recombination will change the subsequent ion charge state substantially. The difference obtained for the measured stopping power of the hydrogen plasma to the maximum theoretical values (Fig. 17) can be understood as a reduced effective ion charge $Z_{eff} \cong 5.5$, due to the presence of a small fraction of neutral gas (about 1%) in the plasma. This explanation is supported by the ionization degree obtained from the plasma diagnostic. Thus, in the framework of an accepted SSM theoretical model, the measurement of stopping power at low beam velocities provides a new tool to determine the ionization degree of a plasma.

In summary, those experimental results demonstrate, the extreme enhancement of the stopping power of low-velocity heavy ions in a fully ionized plasma. In comparison to experimental and theoretical cold gas data, this is an enhancement factor of 35. The effect observed in this experiment is larger by 1 order of magnitude than any other result of plasma stopping power that has been reported previously. In the energy regime below 100 keV/u considered here, these results are close to the expected maximum energy loss in fully ionized hydrogen plasma, where these measurements provide a definitive experimental test of established stopping power models. In this energy regime an enhanced ion charge state compared to cold matter causes the main contribution to produce the large energy loss. A fully ionized plasma target may well be exploited as an effective plama stripper for heavy ion accelerators [34],
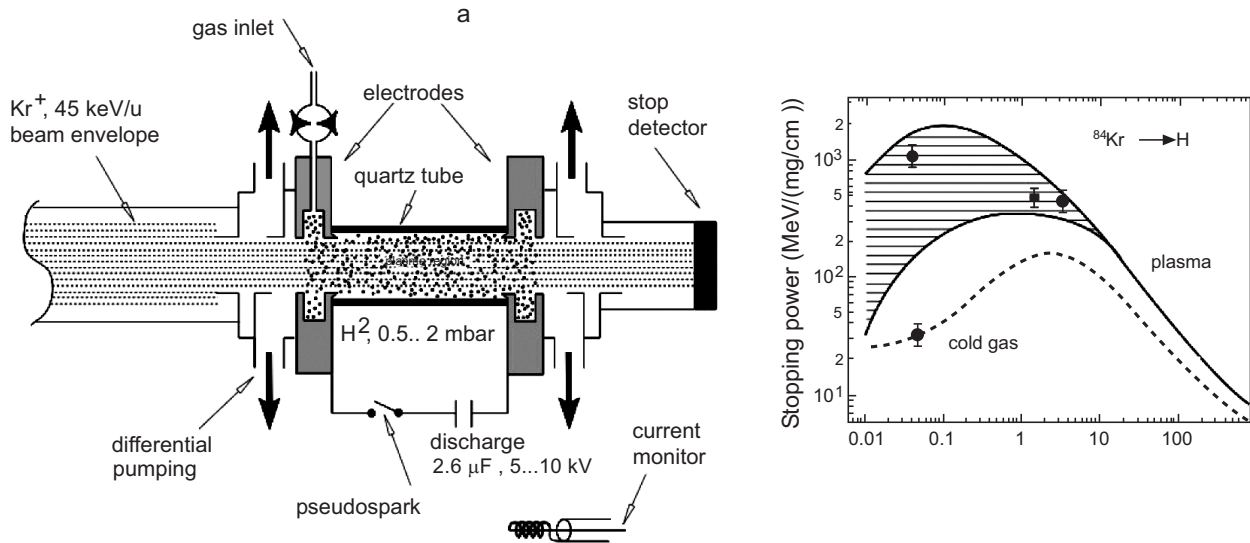
Fig. (17). Stopping power experiment of Maxilac (Jacoby *et al.* [33]). (**a**) Schematic setup; (**b**) Experimental results for the stopping power of a hydrogen plasma and cold hydrogen gas in comparison with theoretical calculations.

since the projectile ion charge states are far above the equilibrium charge states in cold, neutral gas.

7.2. Oxygen in LiH and Plastics

Laser ablated targets allow to explore a much higher temperature regime than previously. As said above (see Sec. 5.2), laser ionization of nonhydrogenic surfaces is seldom complete. Then it appears convenient to switch from the quantum-mechanical Bethelike SSM expression for ion stopping to the classical Bohrlike [35]

$$-\frac{dE}{dx} = -\frac{4\pi Z_{eff}^2}{m\,v_p^2}\left[N_{be}\,\ln\left(\frac{Cm v_p^3}{Z_{eff}e^2\omega_p}\right)\right], \quad C=1.123 \qquad (40)$$

in terms of m, electron mass. N_{be} and N_{fe} refer respectively to the number densities of bound and free electrons. $\hbar\omega_e$ and $\hbar\omega_p$ designate their respective target binding energy.

7.2.1. Experiments

Low-energy heavy ions are generated with the 1.7 MV tandem at Tokyo Institute of Technology [36] (Fig. **18a**) shows a schematic layout of the tandem beam line. The tandem was equipped with a sputter ion source and a PIG ion source for generation of metallic ions and gaseous ions, respectively. In this study one considers mostly oxygen and proton beams. Two types of plasma targets have been installed on the beam line. One was based on a CO_2 laser of 6 J per pulse which irradiated a polyethylene plate or lithium layer with a focusing spot of 9mm × 1mm with longer axis along the incident ion beam [36, 37]. A fresh surface was exposed to the laser (Fig. **18a**) by rotating the plate after every shot. One can operate this plasma source without breaking the vaccum. Ablation mass of the polyethylene was in average 19 µg per shot. The velocity of ablating plasma measured with a biased charge collector was 3.6×10^4 ms^{-1}. The time-resolved optical spectroscopy is carried out using a monochromator of f = 250 mm combined with a streak camera. The electron density of the polyethylene plasma is deduced from the Stark broadening of hydrogen H_α line of

656.3 nm. The electron density at 0.5 mm distance from cold target ranged between 2 and 10×10^{17} cm^{-3}. This density multiplied by a target thickness of 9 mm gave a mass thickness of 1.5 to 7.5 µcm^{-2}. Measurement of electron density was restricted to a time range t > 200 ns because the continuum was dominant over the H_α line. A DC beam of 2.4 MeV O^{2+} was injected into the expanding plasma. The beam is collimated with an aperture of 1 mm in diameter placed 2 cm upstream to the plasma target. A typical beam current on the target was 75 nA, corresponding to 2300 incident ions in a time window of 10 ns. The ions outgoing from the plasma target were analyzed with a dipole magnet and then detected simultaneously with three plastic scintillators of NE102A, which were placed on focal points of the oxygen ions with 2, 4 and 6 charges. The finite flight time of the oxygen ions, i.e., 240 ns for 1.3 m distance, was corrected for the time scale of ion detection.

7.2.2. Results

A. Polyethylene

Fig. (**18b**) shows energy losses of oxygen ions outgoing with charges of 6 and 4 and the time evolution of the electron density of the polyethylene plasma. Both peaks in the energy-loss profiles around 150 ns coincide with the fast spike of the CO_2 laser. Moreover, the energy-loss profiles almost retrace the electron-density profile. The second peaks in these profiles were formed by the CO_2 laser tail. However, the formation mechanism of second peaks stronger than first peaks is not yet fully understood.

EPS is not obvious in a polyethylene plasma with a low degree of ionization. It is interesting to notice that the energy loss data for both charge states indicate similar time profiles although the 6^+ yield was only a few % of the 4^+ yield at t > 200 ns. Similar energy losses might result from almost the same effective charge of the ion projectiles inside the plasma. This fact suggests that the charge state of the outgoing ion might be determined when it has already excited the plasma target.
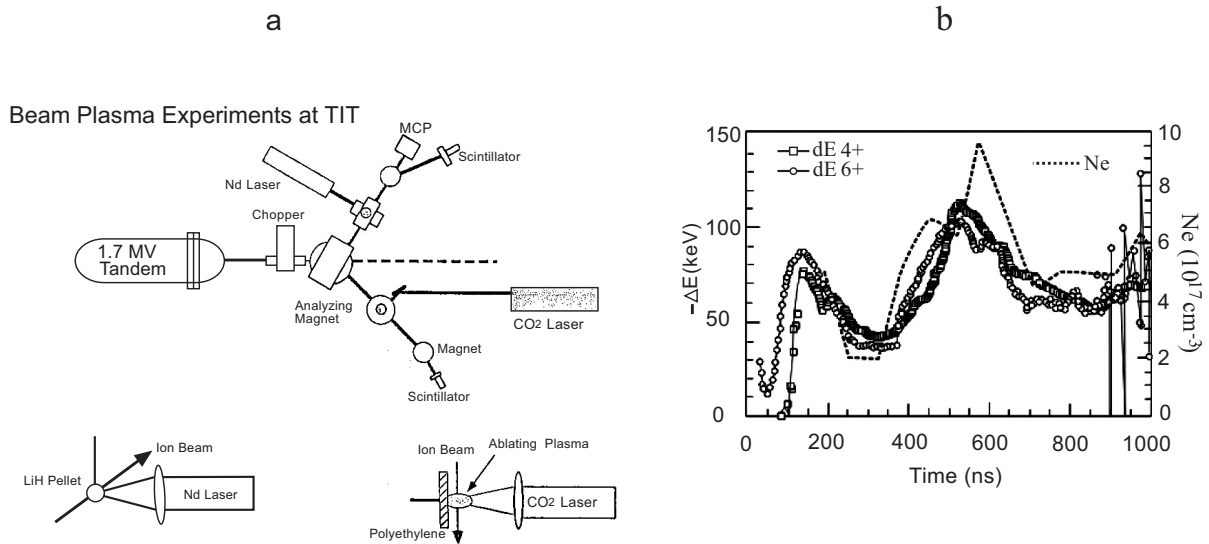
a   b

Fig. (18). Experimental setup for the laser-produced plasma target system at TIT (**a**) O^{n+} in laser ablated plasma (TIT) (**b**) Energy-loss data for outgoing ions of O^{4+} and O^{6+} together with electron density observed for polyethylene plasma. Energy of incident oxygen is 2.4 MeV (Oguri *et al.* [36]).

8. FAST PROTONS ENERGY LOSS

Up to now we have extensively documented the enhanced plasma stopping of arbitrarily charged ions in the (0.05-0.1) MeV/amu energy range interacting with hydrogenic and nonhydrogenic targets, as well. The resulting EPS always appeared as a combination of Coulomb logarithms and projectile effective charge $(Z_{eff}(V_p))$ contributions. In every considered interaction geometry, a suitable modeling has been used to unambiguously identify the EPS source. Now, we explicitly turn to an à priori drastic simplifications of the above pattern. We consider the stopping of protons in the MeV energy range interacting with a strongly ionized hydrogen target. So, excepted in the nearly negligible final phase ($V_p << V_{the}$), the ion projectile retains $Z_{eff}(V_p) = 1$ in cold gas and hot plasma, as well. Then, we can concentrate attention on the relative stopping contribution of bound and free electrons in target.

This apparently simpler case has not been treated at the outset in view of the technological sophistications required for its experimental implementation [38, 39]. A first difficulty arises from scaling rule (9). The SPQR2 setup with $n_e \sim$ a few 10^{17} cm^{-3} demands a proton beam energy in the MeV range. This is a rather low energy for operating a tandem Van de Graaf in stable conditions.

Also, in view of the constant ~ 1 proton charge, the resulting reduced EPS requires a very accurate ion beam spectrometry through adequate proton induced nuclear reactions with very well defined energy thresholds.

Adapting the above SSM expression (20) to the present situation, we can put it under the form

$$-dE = const\,(L_{bep}n_{bep}dx + L_{fe}n_{fe}dx)\,, \qquad (41a)$$

with

$$L_{bep} = \ell n \frac{2m_e V_p^2}{\hbar \varpi} \text{ and } L_{fe} = \ell n \frac{2m_e V_p^2}{\hbar \omega_p}\,, \qquad (41b)$$

where

$n_{bep} =$ bound electron concentration in partially ionized plasma target.

$n_{fe} =$ concentration of free electrons in plasma target.

Considering a cold plasma target including H_2 molecules, one has $\hbar\varpi = 18.5$ eV.

8.1. Experimental Setup

To ensure correct experimental measurements of the Coulomb logarithm within a $\leq 10\%$ error bar, the following important requirements regarding the plasma target, the diagnostics. and the beam stability are to be fulfilled.

(1)   The energy loss dE in the target remains smaller than the initial projectile energy E and, at the same time, exceeds by at least a factor of 10 the stability limit δE for the beam energy provided by the accelerator. Also, the energy loss should significantly exceed the resolution threshold, of the energy analyzing apparatus. For 1-MeV proton, Eqs (41a,b) show that a hydrogen gas target with an areal density of $n_H dx \cong n_e dx \sim 10^{18}$ cm^{-2} is a suitable choice.

(2)   Since l-MeV protons, passing through a hydrogen target with this areal density would lose some 3 keV of their energy, the energy stability of the beam has to be about $\delta E/E \sim \pm 100$ eV/(1 MeV) $\sim \pm l \times 10^{-4}$.

(3)   The energy resolution of the beam energy diagnostics line should be not worse than 10% of the energy loss. In practice a 200 eV resolution has been achieved.

The requirements for the ion beam have been fulfilled by using the UKP-2 tandem accelerator at the Kazakh Institute for Nuclear Physics in Almaty. During the experiments, the

stability of the accelerating voltage was maintained at ±100 V level [38].

The plasma target was integrated into the high vacuum system of the beam line. Differential pumping at a rate of 300 l/s proved to be sufficient in insulating the vacuum beam line from the pressured target during its operating cycle.

The plasma was generated by igniting an electric discharge in two collinear quartz tubes, each of 6 mm in diameter and 78 mm long (see Fig. **19**).

The capacitor bank of 3 μF, discharged at voltages 2-4 kV, produces the electric current of 3 kA flowing in two opposite directions in either of the two quartz tubes. Such a design for the plasma target enables us to suppress the well-known effect of the plasma lens caused by the magnetic field of the current: the focusing effect of the first discharge tube is then compensated for by the defocusing effect of the second one. Symmetry of the discharge is ensured by special inductive coils, included into the discharge circuit, with two wires for the two current branches winded in the opposite directions. For the initial pressure of the hydrogen gas ranging from 200 to 900 Pa (2-9 mbar), a plasma electron density up to 10^{17} cm^{-3} can be produced in such a discharge.
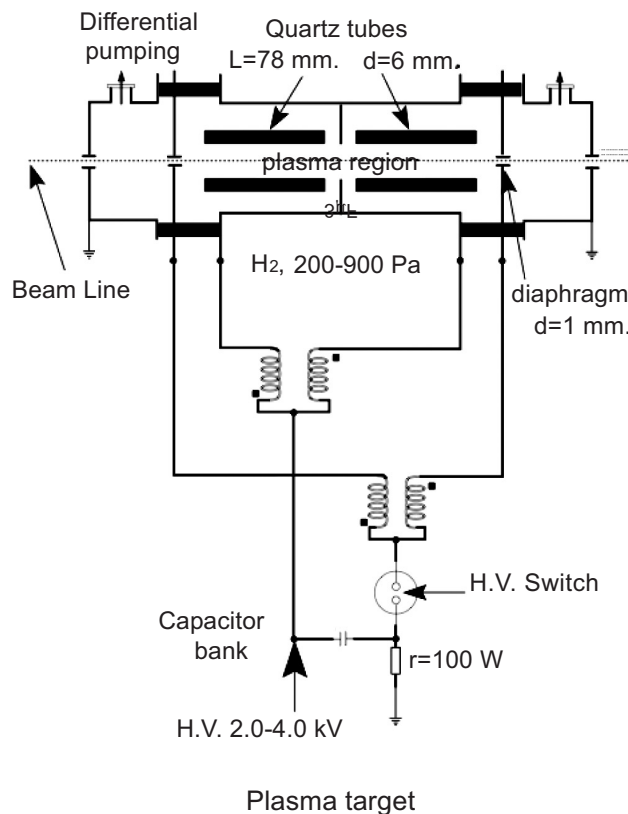

Plasma target

Fig. (19). Principal scheme of the plasma target used for proton stopping (Belyaev *et al.* [38]).

The discharge current oscillates with a half period of ∼ 5 μs, which agrees fairly well with the calculated lifetime of the hydrogen plasma, spilling out of the tube ends in the course of the hydrodynamic expansion.

According to Eqs (41a,b) the essential parameters to be measured in the experiment are the areal density of the free

electrons and the degree of ionization. The measurements have been performed by using the method of time-resolved two-wavelength Mach-Zehnder interferometry in axial direction. Only the plasma region where the proton beam passes —i.e., the region of 1 mm in diameter and 150 mm long— has been probed. The electron areal density in this region is assumed to remain independent of radius, as confirmed by the parallel lines of the interferometric pattern in the streak images.

8.2. Energy-Loss Diagnostics

To carry out measurements of the proton energy losses, the following diagnostic system has been developed. The diagnostic line, consists of the following sequence of the beam-optics elements positioned along the proton beam path behind the plasma target: the entrance slit S1, the bending magnet with a deflection of 45° over the radius of 1.5 m, the electrostatic deflector, which deflects the beam in the horizontal plane, and the quadrupole electrostatic lens. Behind the 0.1 mm slit S2 that can be shifted perpendicular to the incoming beam a 1mm-thick plastic scintillator is placed. The scintillator is connected to a photomultiplier by the fiber optics. The signals are digitized with the 10 MHz analog-to-digital converter and stored in the computer.

In the present experiment the diagnostic line with the L=450 cm separation between the slits S1 and S2 was used, which yields a high-energy resolution δE/E≈0.02% at E = 1 MeV.

To determine experimentally the relationship between the deflection potential U and the energy loss dE, one uses the resonant reaction ^{27}Aℓ (p,γ) → ^{28}Si (E$_r$ = 991.9$^{±}$0.05 keV) are regularly available at the UKP-2 accelerator. The γ photons are detected with a NaI (Tl) scintillator. Proton energy variations caused by variations of the hydrogen gas pressure are compensated for by an appropriate voltage applied to the casing of the ^{27}Aℓ target; this voltage served as a measure of the proton energy loss dE.

Each measurement of the proton energy loss dE in the plasma is performed on measuring the intensity of the proton beam during the discharge at a fixed value of the deflector potential U. The beam current fluctuations due to the instability of the proton source is suppressed by averaging over a series of 50 shots. Then, the measurement was repeated for the next value of the deflector potential U, with an increment corresponding to a dE ≈ 560 eV change in the proton energy. In this way, the entire relevant range of the proton energies was scanned for fixed values of the initial hydrogen pressure and the capacitor bank voltage.

8.3. Results

From Eqs. (41a,b) we get the ratio between Coulomb logarithms for free and bound electrons as

$$\frac{L_{fe}}{L_{bec}} = \frac{dE_p}{dE_c^*} - \frac{1-\alpha}{\alpha}\frac{L_{bep}}{L_{bec}},\qquad(42)$$

where dE_p = 3.8 ± 0.4 keV is the proton energy loss in the plasma target at 1.2 μs after ignition, at maximum ionization α = 0.44 ± 0.1. Here $dE_c^* = dE_c\frac{(n_{fe}dx)}{n_{bec}dx}$ is the energy loss in the cold hydrogen with areal density $n_{bec}dx$ equal to

measured areal density $n_{fe}dx = (7.2 \pm 0.2) \times 10^{17}$ cm^{-2} of free electrons in plasma target.

Finally, evaluating L_{bep} and L_{bec} from Eq. (41b) by substituting $\hbar\varpi = 15.0$ eV and $\hbar\varpi = 18.5$ eV respectively, we arrive at

$$\frac{L_{fe}}{L_{bec}} = 3.1 \pm 0.6 \ , \ L_{fe} = 14.9 \pm 2.8 \tag{43}$$

in convincing agreement with the theoretical expectation

$$L_{fe} = \ell n \frac{2m_e v^2}{\hbar\omega_p}$$

$$= 12.13 + \ell n \left[\left(\frac{E}{1\,\text{MeV}} \right) \left(\frac{10^{17}\,\text{cm}^{-3}}{n_{fe}} \right)^{1/2} \right] \tag{44}$$

$$= 12.48 \ .$$

9. BEYOND SSM

Up to now, we explored many theoretical expectations and possible experimental realisations of the standard stopping model (SSM). Therefore, it is then appropriate to consider further extentions or generalizations allowing to extrapolate it beyond its initial limitations.

9.1. Theoretical Extensions

A first and most obvious inquiry concerns the ion projectile charge state considered as pointlike within the SSM. A so-called GSZ Thomas-Fermi-Like approach [40] could allow for an analytic and efficient inclusion of the extended electron cloud charge distribution at any projectile ionization. Other requested generalizations include higher order in the projectile charge, beyond the squared Bohr-Bethe-Bloch stopping term, as well as arbitrary target ionization.

This last point is strongly emphasized by the timely and mostly significant warm dense matter (WDM) targets [41-42] exhibiting strongly coupled ion plasmas neutralized by arbitrary degenerate electron fluid. When exposed to intense and relativistic heavy ion beams [42]. These targets yield the largest volumes ~ mm^3 of homogeneously heated and strongly coupled plasma, limited by the smoothes density gradients. A preliminary metrological step in this direction is illustrated by the constrained theory-experience confrontation worked out by Chabot *et al*. [43], who consider correlated charge and energy loss measurements in the collisional system Cl ions (1.5 Mev/u) in H$_2$. A windowless gaseous target with different thicknesses was used to measure simultaneously the charge state distributions (CSD) and the energy losses by main populated outgoing charge states (q = 12-15). The Markov chain of the charge-changing process was deduced from a Monte-Carlo computation of the CSD evolution. The stopping cross-section for individual charge states were finally deduced from energy loss data. Comparison of the experimental results with detailed calculations gives a clear evidence of relative importance of the individual contribution of non-linear correction terms and of the electron cloud bound to the projectiles. These two effects may be important for HI-ICF

scenarios where a non-equilibrium charge state behavior is likely occur.

More generally, it appears highly rewarding to contrast SSM predictions essentially valid at weak projectile-target electromagnetic coupling with a more global kinetic approach (CKLT) [44] able to include arbitrary strong coupling at any target ionization degree. The latter elaborates on the well-know convergent kinetic formalism due to Gould and DeWitt [45].

The stopping power of swift heavy ions in both cold and plasma targets. Is expressed by a single formula from which the standard classical or quantum results are retrieved as specific limits. It is based on a modified Bloch correction term devoted to correctly describe the close collisions contribution to the energy-loss process. This correction term is obtained from the convergent kinetic theory (CKT) derived by Gould and DeWitt [45] for calculating transport coefficients in dense plasmas. The CKT is adapted to neutral targets by using the scaling properties of Debye potentials demonstrated by Lindhard. The resulting CKLT stopping expression can be applied to partially ionized heavy ions with a non-Coulomb electron-ion interaction potential. The differences between the CKLT and standard stopping models are investigated in the binary approximation, where the CKLT formula yields the exact result. The usefulness of the CKLT procedure in stopping power applications is then demonstrated using the spherical harmonic oscillator as a target model. The validity domain of the CKLT is analyzed by comparing the results derived by adding the close collision correction term either to the first Born result or to a classical calculation. The classical result is retrieved following during a collision, the time evolution of the Wigner distribution.

In contast to the SSM, the CKLT modeling provides also low ion velocity stopping whenever the projectile-target coupling does not get too large. At low couling, SSM and CKLT match each other. CKLT does not include nonlinear plasma screening effects, neither charge-exchange contribution in cold targets. The latter can turm rather high at low projectile velocity low v_p. Let us also notice a low v_p possible extension of the SSM within a target dielectric picture endowed with a target dielectric picture endowed with binary ionic mixtures (BIM) such as DT in inertial fusion or proton-Fe^{24+} in the solar core [46]. Moreover, very low v_p stopping has been very recently considered in strongly magnetized targets [47].

9.2. Cryogenic Crystal Targets [48]

Basic processes in the targets include isochoric heating by energy deposition of the ion beam in the target, isentropic expansion of target matter under high pressure and compression and heating in single or multiple shocks. The targets can therefore be divided into two different types. In the so called volume targets the ion beam heats the matter directly. Providing short beam pulses this takes place at constant target density. Only after the heating has ceased isentropic expansion sets in. Therefore in this kind of target matter under high pressure at solid state density or below is produced. In the second type of target, the so called compound targets, the ion beam deposits its energy in one part of the target and the expansion of the heated matter then

compresses another part of the target, possibly releasing single or multiple shocks. Single shocks can create high pressures at up to a proximately four times solid state density, whereas in multiple shocks even higher densities can be reached.

In order to achieve high specific energy deposition the requirements on the accelerator are as follows: The number of ions per pulse has to be large. The atomic number of the beam ions must be high since the stopping power is quadratically proportional to the effective charge of the ions in the target. Not only the length of the volume in which the beam energy is deposited should be small but also its width. Fine focusing with a precision plasma lens is therefore crucial. Finally the temporal width of the beam pulse must not exceed the time during which expansion occurs in order to avoid lowering of pressure and stopping power.

A diffuse backlighter flash and a fast framing camera are installed with their optical axis perpendicular to the beam axis for the shadowgraphy measurements. A VUV spectrometer and a fiber optical link to a spectrometer working in the visible range provide information on the self emission of the ion beam heated target. A pulsed magnetic ion spectrometer measures the energy of the beam ions after passage through the target for all experiments where the ion beam is not completely stopped in the target.

Optically clear cryogenic crystals of Xe, Kr, Ar, Ne, deuterium and hydrogen were produced and used as targets for the ion beam. 1 mm thick lead sheets with the surface parallel to the beam axis and lead cylinders 17 mm in diameter were also irradiated.

In the shadowgraphy the expansion of the target material was measured and expansion velocities up to 290m/s perpendicular to the surface of the lead sheet were inferred.

9.3. Aerogel Targets

O.N. Rosmej *et al.* [49] have recently developed cold and very low density S_iO_2 targets.

Aerogel targets of S_iO_2 with a low mean density of 0.15 g/cm^3 allowed extending the ion stopping length more than 10 times as compared to a solid quartz target and it was therefore possible to increase the spatial resolution of the method.

K-shell projectile spectra show the long-lasting radiation of highly charged Ar ions with charges states q = 17, 16 and 15 as well as the radiation from unresolved charge states with q < 15 down to the energy range of 2 MeV/u. The fact that the high charge states are obviously preserved down to very low energies is in disagreement with measurements of the ion charge state distribution measured after passing through solid carbon foils. In these measurements, the charge state is measured with detectors far away from the last interaction process, whereas the current method allows observing the charge state *in situ*. With these new measurements and the new technique, it will be possible to address the question why the charge state distribution of ions measured behind a gaseous target or a solid foil are so different, while the specific energy loss does not differ significantly.

K-shell radiation of fast heavy ions penetrating solid matter was used to analyze the stopping dynamics of ions over more than 80% of the stopping path. The most important advantage of this method is that the data is obtained with a high spatial resolution directly from the interaction volume. In experiments 11.4 MeV/u Ca projectile were slowed down in solid quartz and low-density S_iO_2 aerogel targets. Characteristic projectile and target spectra in the photon energy range of 1.5-4 keV were registered by means of spherically bent crystal spectrometers with high spectral and spatial resolution in the direction of the ion beam propagation. K-shell spectra of heavy ions induced by close collisions with target atoms provided information about the projectile charge state and velocity dynamics. The line intensity distribution of the K-shell transitions arising from ions with different ion charges represents the charge state distribution along the ion beam track. The variation of the line Doppler shift due to the ions deceleration in the target material was used to determine the ion velocity dynamics. The spectroscopic analysis of the stopping process was complemented by measurements of the energy loss and ion charge state distribution after the ion beam emerged from the target using a standard time-of-flight methods and magnet spectrometer.

It should be appreciated that aerogel targets document methods for space resolved measurements of the fast heavy ion velocity during the interaction with matter are presented. The main idea is to use the characteristic radiation from ions traveling in the stopping media undergoes a Doppler shift, while varies along the ion beam trajectory due to the ion deceleration. High spectrally ($\lambda/\Delta\lambda$= 1000-3000) and spatially (up to 30-100 mum) resolved X-ray K-shell spectra of Ca projectile ions as well as of the ionized stopping media have been obtained using focusing spectrometers with spatial resolution (FSSR). Spherically bent crystals of quartz and mica with small curvature radii R = 150 mm and large apertures (15 x 50 mm) have been used as dispersive elements. Fast Ca^{+6} ions with energies of 5.9 and 11.4 MeV/u were stopped in quartz. S_iO^2 aerogels and CaF^2 targets. High spectral and spatial resolution of the spectra allowes measuring the velocity of heavy projectile ions at different points along the beam trajectory. A method based on the utilization of two equal spectrometers at different angles of observation (along and downstream the ion beam propagation direction) is proposed to measure the absolute values of ion velocity inside the stopping media. The use of aerogel targets with extremely low volume density (0.15 g/cc) increases the ion stopping range up to 50 times in comparison to solid quartz. This provides the resolution of the stopping process dynamics. Experimentally it was found that Ca^{+6} ions with the initial energies of 5.9 or 11.4 MeV/u propagate in solid dense matter as Ca^{+17}-Ca^{+19} down to the energies of 2.0-2.2 MeV/u.

9.4. Explosively Driven Plasma Target

To investigate the heating of matter by particle beams detailed knowledge of the energy loss in dense plasma at high pressures and temperatures is crucial. With increasing plasma density the influence of the effects of the Coulomb coupling is expected to be of great significance. Shock wave techniques make it possible to produce plasmas with electron

densities of up to $n_e \sim 10^{22}$ cm^{-3}. Toward this goal explosively driven plasma generators have been developed [50]. In such devices plasma is created behind the plane front of an intense shock wave generated by the detonation. of high explosive chemicals. Standard shock wave plasma generators contain more than 500 g of high explosives, to produce shock compressed strongly coupled plasma with temperatures of 1-10 eV, pressures of 1-200 kbar and Coulomb coupling parameters of 1-5. Explosively driven plasma targets look very attractive for beam plasma interaction experiments because of the absence of strong electromagnetic fields like in discharges, which affect significantly the beam transport.

To use standard explosive devices in beam areas of accelerator facilities it is necessary to build large-scaled explosive chambers and to solve the problems of matching high vacuum beam lines with the explosive apparatus.

To protect the equipment from the debris of the exploding plasma generator, it is placed into a special compact vacuum pumped (up to 10^{-2} Torr) steel chamber with a diameter of 80 cm. The chamber allows to apply explosive charges of up to 150 g of TNT and is specially designed to provide a complete matching with the beam line of the accelerator facility.

As a first step one uses small charge (< 150 g TNT) explosive generators in a vacuum pumped explosive metallic chamber with fast valves in such experiments. To optimize the explosive plasma generators numerical simulations of plasma shock compression and a special series of shock wave experiments were carried out. They show the possibility to construct small-sized linear and cumulative explosively driven generators with shock front velocities of about 6-20 km/s having a high explosive charge not exceeding 30-150 g. Using these devices one can investigate experimentally (i) the effect of strong, interparticle interactions in plasma on the energy loss of fast ions and (ii) the stopping power of plasma at high ionisation degrees.

Computer simulations of explosively driven plasmas show that using the simplest (linear) scheme of shock tube makes it possible to obtain an ionization degree $\alpha \sim 1$ and high electron densities for gases with a rather high molecular weight. For example, shock waves with a velocity of 6 km/s in xenon at an initial pressure of 1 bar produce a plasma with an electron density of more than $n_e \sim 10^{20}$ cm^{-3} and an ionization degree of about $\alpha \sim 1$. Higher plasma densities can be reached without any problem by increasing the initial pressure of the investigated gas.

Very recently K. Weyrich *et al.* [51] have determined energy loss and charge state distribution of C, Ar and Xe at 5.9 MeV/nucleon, interacting with a shock driven.

Ar gas target qualified by:

- Free electron densities between $3*10^{19}$ and $1.5*10^{20}$ cm^{-3}.

- Electron temperatures ~ 2.0 eV.

- Compression factors of 8-10 (pressure in the plasma phase/initial gas pressure).

- Γ-Parameters between 0.55 and 1.5.

- Ionization degree in the plasma 50-30%.

10. CONCLUSIONS AND OUTLOOK

We have essentially demonstrated how the most economical extension of the so-called linear Bohr-Bethe-Bloch (3B) formalism for nonrelativistic ion stopping in cold matter (gases, solids) may be worked out for arbitrarily ionized targets. A specific emphasis has been given to the ion projectile inflight effective charge $Z_{eff}(V_p)$ through its interactions with target electrons.

Within the framework of the standard stopping model (SSM) based on the Born-RPA approximation for the projectile ion-target electron coupling, enhanced ion stopping relative to cold matter equivalent is thus expected. It is essentially documented by the more flexible response of target free electrons to the incoming ion electrostatic potential compared to the bound electrons one. Amongst the latter, weakly bound ones should also provide a significant stopping efficiency.

As a consequence a fully ionized target is expected to provide the highest ion stopping effect because of a highest $Z_{eff}(V_p)$ (vanishing recombination) and most efficient free electron stopping.

On the experimental side, we stressed at length, through relevant sum rules, the requested methodology for synchronizing an intrinsically transient plasma target with the incoming ion beam time structure. Most of the considered accelerating structures are taken linear (Tandem/Van De Graaf, RFQ, Alvarez, etc…).

We focussed attention on accurate on-line analysis of plasma parameters: particle densities and temperature, ionization degree, thermodynamical state.

One of the most promising outputs of this endeavour is the possibility of building a robust and significant data basis for driven-pellet interaction of interest for particle-driven inertial confinement fusion (ICF). For instance, the feasibility of compressing a deuterium + tritium filled capsule through a few MJ of intense (10 kA) heavy ion beams has thus been clearly demonstrated [52].

Considering altogether the presently documented enhanced ion stopping in hot target which features an improved driver pellet coupling with the robustness, high repetition rates of heavy ion accelerating structures, and higher power-driver conversion efficiency leads us to objectively qualify intense heavy ion beams as the best ICF driver. Beyond this highly promising outlook, one should also pay a due attention to the potentialities of intense and low energy ion beams for selective target heating in order to process materials. For instance, Yatsui *et al.* [53] have successfully mastered the light ion driven ablation of metallic surfaces to depositing carefully monolayers on another facing plate.

In the same vein, the highly promising prospects of target heating through PW-laser produced intense proton or heavier ions open a rather bright future for particle driven ICF and warm dense matter production, as well.

This explains that to address the many other applications of intense ion beam interaction with hot target a thorough

examination of high order corrections to the SSM is requested for asserting realistically the ion projectile-target electron coupling as outlined in Sec. 9.1. Similarly, strong Coulombic coupling effects in the heated target should also be given a due attention.

REFERENCES

[1] Uehling EA. Penetration of heavy charged particles in matter. Annu Rev Nucl Sci 1954; 4: 315-50

[2] Fano U. Penetration of protons, alpha particles and mesons. Ann Rev Nucl Sci 1963; 13: 1-66; Northcliffe LC. Passage of heavy ions through matter. Annu Rev Nucl Sci 1963; 13: 67-102

[3] Keefe D. Inertial confinement fusion. Annu Rev Nucl Sci 1982; 32: 391-441

[4] Bangerter RO. Targets for heavy-ion fusion. Fus Technol 1988; 13: 348-55

[5] Wei Yu, Buchenkov V, Sentoku Y, et al. Electron acceleration by a short relativistic laser pulse at the front of solid targets. Phys Rev Lett 2000; 85: 570-3

[6] Ferrari A. Modeling extragalactic jets. Annu Rev Astron1998; 36: 539-98

[7] Young FC, Mosher D, Stephanakis SJ, et al. Measurements of enhanced stopping of 1-4 MeV deuterons in target-ablation plasmas Phys Rev Lett 1982; 49: 549-53

[8] Mehlhorn TA. A finite temperature model for ion energy deposition in ion-driver inertial confinement fusion targets. J Appl Phys 1981; 52: 6522-32; Long KA, Tahir NA. Theory and calculation of the energy loss of charged-particles in inertial fusion plasmas. Nucl Fusion 1986; 26: 555-91

[9] Deutsch C. Ion and cluster ion-plasma interaction for particle-driven fusion. Plasma Phys Control Fusion 1999; 41: A195-206 and also Deutsch C. Inertial confinement fusion driven by intense ion beams. Ann Phys (Paris) 1986; 11: 1-111

[10] Maynard G, Deutsch C. Energy loss and straggling of ions at any velocity in dense plamsas at any temperature. Phys Rev 1982; A26: 665-8 and Erratum 1983; A27: 574(E).

[11] Meyer-Ter-Vehn J, Witkowski S, Bock R, et al. Accelerator and target studies for heavy ion fusion et GSI. Phys Fluids 1990; B 2: 1313-7

[12] Maynard G, Deutsch C. Born RPA approximation for ion stopping in arbitrary degenerate electron fluid. J Phys (Paris)1985; 46: 1113-22

[13] Deutsch C, Maynard G. Stopping of pointlike charges in a dense electron fluid. Recent Res Dev Plasmas 2000; 1: 1-23 and also Arista NR, Brandt W. Energy loss and straggling of charged particles in plasmas at all degenaracies. Phys Rev 1981; A 23: 1898-905

[14] Zwicknagel G, Toeppfer C, Reinhard PG. Stopping of heavy ions at strong coupling. Phys Rep 1999; 309: 117-208

[15] Deutsch C. Nodal expansion for a real matter plasma. Phys Lett 1977; 60A: 317-8

[16] Bohr N. On the theory of the decrease of velocity of moving electrified particles on passing through matter. Philos Mag 1913; 25: 10

[17] Fermi E. The ionization loss of energy in gases and condensed materials. Phys Rev 1940; 57: 485-93.

[18] Deutsch C, Maynard G, Bimbot R, et al. Ion beam-plasma interaction: a standard model approach. Nucl Instrum Methods 1989; A278: 38-43

[19] Bell GI. The capture and loss of electrons by fission fragments. Phys Rev 1953; 90: 548-57

[20] Hewett DW, Kruer WL, Bangerter RO. Corona plasma instabiliries in heavy ion fusion. Nucl Fusion 1991; 31: 431-46

[21] Gardès D, Servajean A, Kubica B, et al. Stopping of multicharged ions in dense and fully ionized hydrogen. Phys Rev 1992; A46: 5101-11

[22] Betz HD. In: Datz S, Ed. Applied atomic collision physics. New York: Academic Press 1983; vol. 4: pp. 1-30.

[23] Nardi E, Zinamon Z. Charge state and slowing down of fast ions in Plasmas. Phys Rev Lett 1982; 49: 1251-4

[24] Maynard G, Deutsch C. Interaction of heavy ions with gas and plasma targets. J Phys (Paris) 1988; 49: C7-89-97

[25] Mosher D, Cooperstein G, Stephankis SJ, Goldstein S, Colombant DJ, Lee R. Memorandum report 3658, Naval Research Laboratory 1977.

[26] Zinamon Z. In: Velarde G, Ronen Y, Martinez-Val JM, Eds. Nuclear Fusion by Inertial confinement. Boca Raton: CRC Press, 1993; pp. 119-28

[27] Toner W. Alpha-particle measurements of stopping power in hot dense materials, Proceed 2nd International workshop Atomic physics for ion-driven fusion, Rutherford Lab, September 1984.

[28] Couillaud C, Deicas R, Nardin Ph, et al. Ionization and stopping of heavy ions in dense laser-ablated plasmas. Phys Rev 1994; E49: 1545-62.

[29] Hoffman DHH, Weyrich K, Wahl H, et al. Maurmann S. Experimental observation of enhanced stopping of heavy ions in a hydrogen plasma, Z Phys 1988; A330: 339-340; Hoffman DHH, Weyrich K, Wahl H, Bimbot R, Fleurier C, Gardès D. Energy loss of heavy ions in a plasma targer. Phys Rev 1990; A42: 2313-21.

[30] Neuner U, Ogawa M, Kobayashi H, et al. Interaction of MeV heavy ions with a laser plasma and a Z-pinch helium plasma. Nucl Instrum Methods 1998; A415: 586-90.

[31] Chabot M, Gardès D, Kiener J, et al. Charge-state distributions of chlorine ions interacting with cold gas and fully ionized plasmas. Laser Part Beam 1995; 13: 293-302; Chabot M, Gardès D, Box P, et al. Stripping properties of a plasma medium for MeV/u chlorine ions. Phys Rev 1995; E51: 3504-10.

[32] Maynard G, André W, Chabot M, et al. Charge evolution of swift heavy ions in fusion plasmas. Nuo Cim 1993; 106A: 1825-37.

[33] Jacoby J, Hoffman DHH, Laux W, et al. Stopping of heavy ions in a hydrogen plasma. Phys Rev Lett 1995; 74: 1550-3

[34] Engelbrecht M, Engelhardt MP, Flier HP, et al. Numetical description and development of plasma stripper targets for heayvy-ion beams. Nucl Instrum Methods 1998; A415: 621-7.

[35] Sigmund P. Low speed limit of Bohr's stopping formula. Phys Rev 1996; A54: 3113-7.

[36] Oguri Y, Abe A, Sakumi A, et al. Development of a laser-produced plasma target for beam-plasma interaction researches. Nucl Instrum Methods 1998; A415: 657-61.

[37] Sakumi A, Okazaki H, Watanabe T, et al. Experiments on the interaction of fast heavy ions with a laser-plasma target. Nucl Instrum Methods 1998; A415: 648-52.

[38] Belyaev G, Basko M, Cherkasov A, et al. Measurement of the Coulomb energy loss by fast protons in a plasma target. Phys Rev1996; E53: 2701-7.

[39] Golubev A, Basko M, Fertman A, et al. Dense plasma diagnostics by fast proton beams. Phys Rev 1998; E57: 3363-7.

[40] Deutsch C, Maynard G. Stopping of ions with extended charge distribution in dense matter. Phys Rev1989; A 40: 3209-18.

[41] Fortov VE, Hoffmann DHH, Sharkov B. Intense ion beams for generating extreme states of matter. Phys Usp 2008; 51: 109-31.

[42] Tahir NA, Lomonosov IV, Shutov A, et al. Review of high energy density physics:The HEDgeHOB Collaboration. Nucl Instrum Methods 2009; A 606: 128-33.

[43] Chabot M, Gardès D, Nectoux M, Maynard G, Deutsch C. Energy loss of Clq+(52 MeV) through dilute H2 target: evidence of non-linear term and non-Coulombian potential contribution. Nucl Instrum Methods 2007; A577: 353-6

[44] Maynard G, Zwicknagel G, Deutsch C, Katsonis K. Diffusion-transport cross-section and stopping power of swift heavy ions. Phys Rev 2001; A63: 052903; Maynard G, Deutsch C, Dimitriou K, Katsonis K, Sarrazin M. Evaluation of the energy deposition profile for swift heavy ions in dense plasmas. Nucl Instrum Methods 2002; B 195: 188-215

[45] Gould HA, DeWitt HE. Convergent kinetic equation for a classical plasma. Phys Rev 1967; 155: 68- 74.

[46] Tashev B, Baimbetov F, Deutsch C, Fromy P. Low velocity ion stopping in binary ionic mixtures. Phys Plasmas 2008; 15: 10270-1-10.

[47] Deutsch C, Popoff R. Low ion-velocity slowing down in a strongly magnetized plasma. Phys Rev 2008; E 78: 056405-1-7.

[48] Neuner U, Bock R, Funk UN, et al. Intense heavy ion beams as a tool to produce and analyze dense plasmas. Contrib Plasma Phys 1999; 39: 49-52.

[49] Rosmej ON, Blazevic A, Korostiy S, et al. Charge state and stopping dynamics of fast heavy ions in dense matter. Phys Rev 2005; A72: 052901-1-10; Eisenbarth S, Rosmej ON, Shevelko VP, Blazevic A, Hoffmann DHH. Numerical simulations of the

projectile ion charge difference in solid and gaseous stopping matter. Laser Part Beams 2007; 25: 601-11.

[50]   Mintsev V, Gryaznov V, Kulish M, *et al.* On measurements of stopping power in explosively driven plasma targets. Nucl Instrum Methods 1998; A415: 715-9.

[51]   Weyrich K, Wahl H, Hoffmann DHH, *et al.* Shockwave driven non-ideal plasmas for interaction experiments with heavy ions. J Phys A 2006; A39: 4749-54.

[52]   Deutsch C, Hofman I. Intense ion beams for inertial fusion. Compt Rend (Paris) 2000; 1(IV): 751-8.

[53]   Jiang W, Hashimoto N, Shinkal H, Ohtomo K, Yatsui K. Characteristics of ablation plasmas produced by pulsed light ion beam interaction with targets and application to materials. Nucl Instrum Methods 1998; A415: 533-8.